

We thank the two reviewers for their valuable comments and constructive suggestions on the manuscript. Below, we explain how the comments and suggestions are addressed and make note of the revision in the revised manuscript.

## **Reviewer #1**

*This paper examines the dust cycle simulated by 15 models from the Coupled Model Intercomparison Project (CMIP5). Annual mean dust emission, burden, lifetime, deposition, and surface concentration are examined. Large discrepancies are found in global dust emission and burden, while simulated dust deposition and concentration are within a factor of 10 at most stations. Wet deposition is found to contribute about 12-39% of total dust deposition. Overall, the paper is well organized and results are clearly presented. Further improvements are suggested as follows.*

Reply: We thank the reviewer for his/her detailed review and helpful comments. The text, tables, and figures are revised as the reviewer suggested.

### ***Major comments:***

***1. It is not clear why the MERRA2 is included in CMIP5 model comparisons. It's not a fair comparison since meteorological fields and total AOD in the reanalysis are assimilated with observations, but not in CMIP5 models. Although results from the MERRA2 can provide some insights on how well the dust cycle is captured when meteorological fields are constrained with observations, this aspect is not fully discussed in the paper, e.g., how model biases in meteorological fields, such as surface 10 m wind, precipitation, and atmospheric circulation, in CMIP5 models are transformed to biases in dust simulation. I'd suggest either better justifying why the reanalysis is used and the benefits of such a comparison or removing the comparison with MERRA2 results.***

Reply: We thank the reviewer for pointing out this. Although there are still gaps in dust fields between MERRA-2 reanalysis and observations, MERRA-2 is a state-of-art aerosol reanalysis and provides a global dust distribution which is better constrained by satellite observations. The comparison of CMIP5 models with MERRA-2 will benefit the identification of model discrepancy.

On the other hand, we also note the dust emission in MERRA-2 is less reliable compared to dust burden and concentration as it is not directly adjusted by the assimilation system. Dust emission in MERRA-2 depends not only on meteorological conditions but also on dust emission parameterizations and thus still of large uncertainty. It is a pity that we can't identify the model biases in dust emission in CMIP5 models and thus we are unable to analyze how model biases in meteorological fields, such as surface 10 m wind, precipitation, and atmospheric circulation, in CMIP5 models are

transformed to biases in dust simulation. However, as the development of a referential data is also important for model evaluation, we also mention the limitations when using MERRA-2 data. This will also benefit the development of further dust aerosol reanalysis, for example, by adjoint inversion of dust emission using more specific observations such as lidar observations (Yumimoto et al., 2007).

Because of these benefits, we keep using MERRA-2 to evaluate CMIP5 models. To clarify, in the revised manuscript, we first move the description of MERRA-2 data from Section 2 “Model data” to Section 3.2 “MERRA-2 reanalysis” (under Section 3 “Reference data”). Second, we add more explanations to better justify why MERRA-2 reanalysis is used in Section 3.2: “**Because the station observations are limited in space coverage (Figure 1), we also use the aerosol reanalysis from Modern-Era Retrospective Analysis for Research and Applications, version 2 (MERRA-2) to evaluate the CMIP5 model results.**” (Lines 213-215). Third, we add the discussions on further development of reanalysis data in Section 6: “**It is desirable that future aerosol reanalysis also includes adjoint inversion of dust emissions using more specific observations such as lidar observations as done in Yumimoto et al. (2007)**” (Lines 690-692).

***2. In section 4, some model discrepancies are attributed to potential causes, such as model biases in vegetation cover (lines 312-314), wind speed and precipitation (lines 343-345). I wonder if it’s possible to add analysis to verify these hypotheses by examining a few relevant variables from CMIP5 model output, if available. This will help us better understand the underlying causes of model biases.***

Reply: We thank the reviewer for this helpful suggestion. Following the suggestions, we add more analysis to identify the reasons for model discrepancies.

First, we add the analysis on the bare soil fraction, surface wind speed, and soil moisture in the ACCESS1-0, HadGEM2-CC, and HadGEM2-ES, which have similar dust emission parameterizations. The results show HadGEM2-CC/ES simulate much larger bare soil fraction especially in Australia, North America, and South Asia compared to the International Geosphere-Biosphere Programme (IGBP) data used in ACCESS1.0. HadGEM2-CC/ES also simulate significantly larger surface wind speed in Australia and South Asia. In Australia, HadGEM2-CC/ES also simulate slightly smaller soil moisture. These can explain the excessive dust emission in Australia in HadGEM2-CC/ES than ACCESS1-0. Overestimated bare fraction in South Asia and North America can also explain the excessive dust emission simulated by HadGEM2-CC/ES in these regions.

Second, we also compare the leaf area index, surface wind speed, soil moisture in the four MIROC family models (MIROC4h, MIROC5, MIROC-ESM, MIROC-ESM-CHEM) which adopt similar dust emission parameterizations. Instead of using bare soil fraction directly, MIROC models use leaf area index to determine the vegetation cover empirically for dust emission. The results show compared to MIROC5, MIROC4h

simulates significantly smaller surface wind speed and adopts a larger leaf area index in the dust source regions, which leads to much smaller dust emission in MIROC4h. Compared to MIROC5, MIROC-ESM and MIROC-ESM-CHEM simulates larger leaf area index in Australia, South America and southern Africa, which can largely explain the difference of dust emissions in these regions among MIROC5 and MIROC-ESM/MIROC-ESM-CHEM.

In the revised manuscript, we have demonstrated these results by adding Figures 4 and 5 and revising/adding corresponding statements for the reasons of model discrepancies in Section 4.2:

- a. “The excessive dust emission in Australia from HadGEM2-CC/ES is mainly ascribed to the excessive bare soil fraction simulated by HadGEM2-CC/ES, as indicated by its comparison with International Geosphere-Biosphere Programme (IGBP) data used in ACCESS1-0 (Figure 4a-4c). The overestimation of bare soil fraction in HadGEM2-ES is also illustrated in Collins et al. (2011). In fact, the ACCESS1-0 model that uses the similar dust emission parameterization but with the prescribed vegetation from IGBP simulates a much lower dust emission than HadGEM2-CC/ES. Compared to ACCESS1.0, HadGEM2-CC/ES simulate larger surface wind speed and slightly smaller soil moisture in Australia (Figures 4d-4i), which can also partly explain the larger dust emission in HadGEM2-CC/ES.” (Lines 394-403)
- b. “The low dust emission in Australia from MIROC-ESM and MIROC-ESM-CHEM is related to the prognostic vegetation used for dust emission. As shown in Figure 5a-5d, MIROC-ESM and MIROC-ESM-CHEM simulate much larger leaf area index compared to the two other MIROC family models (MIROC4h and MIROC5).” (Lines 408-411)
- c. “Small dust emission area in MIROC4h may be mainly due to the weaker surface winds in MIROC4h compared to other three MIROC family models (MIROC5, MIROC-ESM, MIROC-ESM-CHEM) (Figure 5e-5f). In the dust source regions (normalized dust emission flux  $>0.01$ ), the annual mean surface wind speeds are 3.7, 4.4, 4.1, and 4.1  $\text{m s}^{-1}$ , respectively in MIROC4h, MIROC5, MIROC-ESM and MIROC-ESM-CHEM. MIROC4h differs much from other three MIROC models in both dynamic core and physical parameterizations (Watanabe et al., 2010, 2011; Sakamoto et al., 2011), which can explain the weakest surface winds in MIROC4h. In North Hemisphere, MIROC4h adopts a larger leaf area index than MIROC5, which can also lead to the smaller dust emission area in MIROC4h (Figure 5a-5b).” (Lines 434-444).

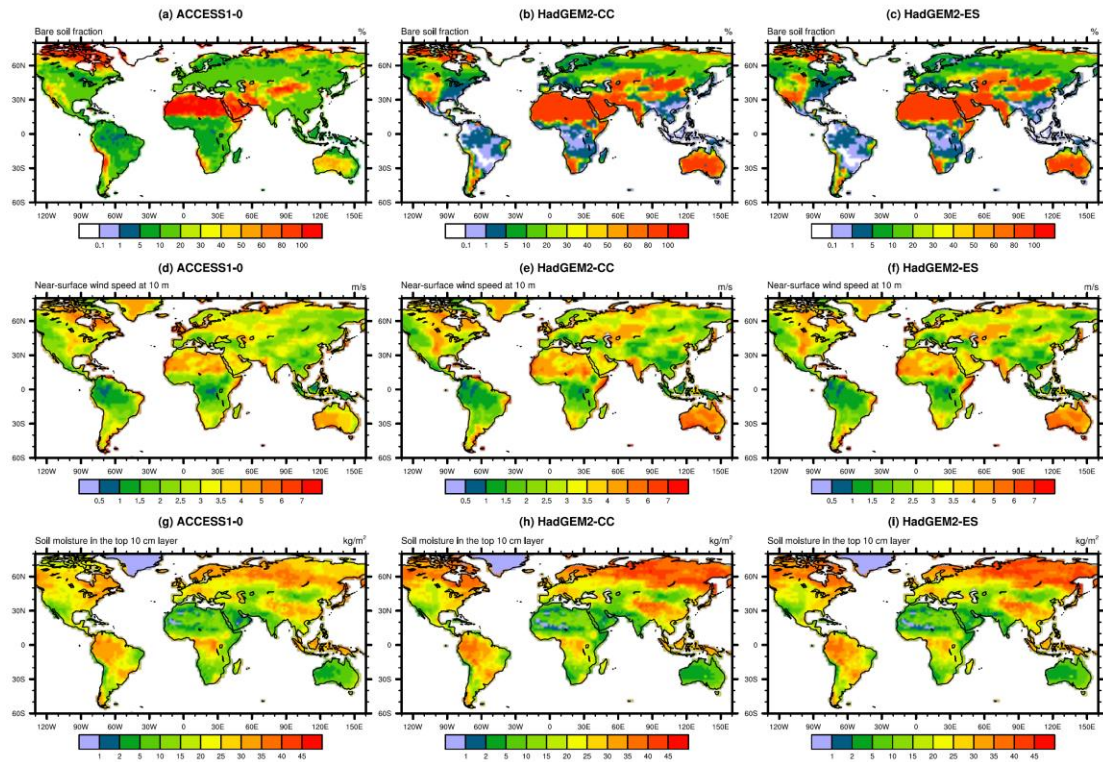


Figure 4. Bare soil fraction (%), near-surface wind speed at 10 m over land ( $\text{m s}^{-1}$ ), soil moisture in the top 10 cm layer ( $\text{kg m}^{-2}$ ) in ACCESS1-0, HadGEM2-CC, and HadGEM2-ES. Note that except bare soil fraction in ACCESS1-0 which is prescribed and set constant for each year, other results are all from model simulations during 1960-2005.

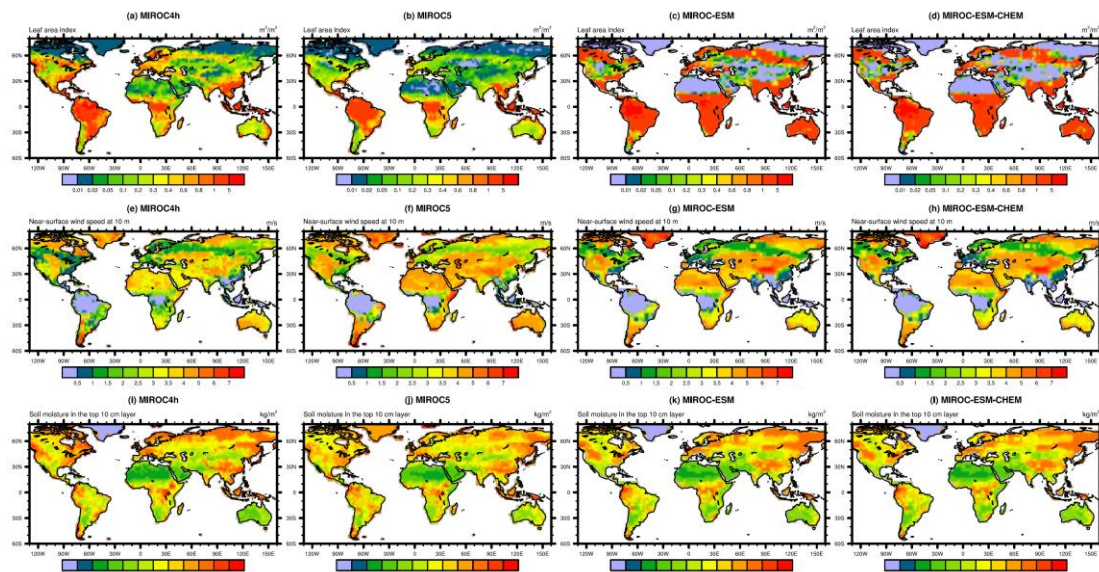


Figure 5. Minimum leaf area index of a calendar year ( $\text{m}^2 \text{m}^{-2}$ ), annual mean surface wind speed at 10m ( $\text{m s}^{-1}$ ), and mean soil moisture in the top 10 cm layer ( $\text{kg m}^{-2}$ ) during 1960-2005 in four MIROC family models. For each grid box, monthly mean leaf area index for each month of a calendar year is first derived based on the average of 1960-2005, and then the minimum of leaf area index among these months (i.e., January to December) is plotted.

**3. Previous studies of dust simulation in CMIP5 models are thoroughly reviewed in the introduction but not in the result section. Please consider adding discussion and comparisons with current findings in the analysis.**

Reply: We thank the reviewer for this good suggestion. The studies of Evan et al. (2014) and Wu et al. (2018b) investigate the dust cycle in specific regions, which can complement our study focusing on dust cycle at global scale. The study of Pu and Ginoux (2018) investigated the dust optical depth in seven CMIP5 models and several of our findings are consistent with theirs. In the revised manuscript, we add discussions on previous studies and comparisons with our study in the result section:

- a. “This result is consistent with Pu and Ginoux (2018) that investigated the global distribution of dust optical depth in seven CMIP5 models.” (Lines 333-335)
- b. “The extent of “dust belt” can be more clearly seen when we zoom in specific regions such as North Africa (Evan et al., 2014) and East Asia (Wu et al., 2018b). For example, in East Asia, although the CMIP5 models can reproduce the dust emissions in the deserts of northern China and southern Mongolia, they differ greatly in the edges of these deserts, with three models (MIROC5, CanESM2, and CSIRO-MK3-6-0) simulating dust emission over Tibetan Plateau and seven models (e.g., ACCESS1-0) simulating dust emission in the southern part of North China (Wu et al., 2018b).” (Lines 348-354)
- c. “The total amount of dust emission in North Africa and East Asia have been presented in Evan et al. (2014) and Wu et al. (2018b), respectively. Here we show the results for all the nine regions in the globe and their comparison.” (Lines 377-

- 379).
- d. “The large scatter of CMIP5 results in North America and Australia is also indicated by dust optical depth, as shown in Pu and Ginoux (2018)” (Lines 388-390)
  - e. “This is also consistent with the overestimation of dust optical depth in Australia by HadGEM2-CC/ES compared to satellite observations (Pu and Ginoux, 2018).” (Lines 551-553)

***Minor comments:***

***1. Section 2, CMIP5 models have different horizontal resolutions. Did you interpolate model results to the same grid for comparison?***

Reply: We interpolate model results to the coarsest resolution among all the models when generating multi-model statistics. To clarify, we add in the revised manuscript: “These models have different horizontal resolutions (Table 1). To generate multi-model statistics of dust emission intensity (Section 4.2), individual model results are interpolated to the coarsest resolution among these models (i.e.,  $2.8^\circ \times 2.8^\circ$ ) using area conserve remapping ([http://www.ncl.ucar.edu/Document/Functions/Contributed/area\\_conserve\\_remap\\_Wrap.shtml](http://www.ncl.ucar.edu/Document/Functions/Contributed/area_conserve_remap_Wrap.shtml), accessed on 6 June 2020).” (Lines 143-148)

***2. Line 118, I don’t think GFDL-CM3 model uses dynamic vegetation to update dust source map. Please double check.***

Reply: We thank the reviewer for pointing out this. We have checked GFDL-CM3 doesn’t use dynamic vegetation to update dust source map. We have corrected this in the text and Table 1.

***3. Line 130, please add “in diameter” after “have the larger size range of 0.0632-63.2  $\mu\text{m}$ ”***

Reply: Done.

***4. Lines 166-167, it seems that dust burden and deposition are not affected by the assimilation of total AOD, right? Please clarify.***

Reply: We thank the reviewer for the comment. The MERRA-2 aerosol reanalysis is generated using the increment analysis update procedure. The procedure first derives the AOD increment and then derives 3-dimensional analysis increment for aerosol mixing ratio. This affects the aerosol burden and thus aerosol deposition, but it doesn’t affect dust emission. To clarify, in the revised manuscript, we add a description about the aerosol assimilation procedure: “The MERRA-2 aerosol reanalysis uses increment analysis update procedure, which derives 3-dimensional analysis increment for aerosol mixing ratio based on the aerosol optical depth (AOD)

analysis increment (Randles et al., 2017). The procedure further affects the aerosol deposition flux.” (Lines 223-226)

**5. Lines 191-196, can you provide how many years of data are available for dust deposition and surface concentration and add the info to Table 2? Deposition data cover "several to hundreds of years", while CMIP5 data are averaged over 1960-2005. Can you add a short discussion on how the inconsistency of data may affect the comparison?**

Reply: We thank the reviewer for a good suggestion. We have examined carefully the periods for the observations used in the study. For surface dust concentration, in the revised manuscript, we have added the information in Table 2.

For the fraction of wet fraction shown in Table 2 in the original manuscript, we find the observation periods were mostly less than 2 years and the observations may be less representative of a climatology. Therefore, in the revised manuscript we don't use the observations for fraction of wet deposition and deleted the comparison results of fraction of wet deposition.

For the deposition flux at 84 stations, the observation periods varied depending on the different observation type. This dataset is directly from AeroCom archive. As some of observation periods were already given in previous studies and the exact periods for ice core data at 5 stations are not available, we prefer to point out these studies to the readers and provide an informative description in the revised manuscript: “**The observation periods varied for different stations. Dust deposition from DIRTMAP is from sediment traps and following Tegen et al. (2002), we only use those 41 stations with deployment period larger than 50 days. Original data of Ginoux et al. (2001) contains both measurements and model estimates. We only use the measurements from Ginoux et al. (2001) which consists of 10 stations and the observation periods varied from 1 to 20 years (see sites # 2, 3, 4, 5, 6, 7, 8, 14, 15, 16 in Table 6 of Ginoux et al. (2001)). Data of Mahowald et al. (1999) was derived from ice core data and consists of 6 stations. Except at one of station (i.e., Renland) where the period was 5 years (i.e., 1813-1819 excluding 1816-1817), the exact observation periods at other 5 stations were not provided and generally covered a time slice of tens of years or more for current climate. In addition, Mahowald et al. (2009) further compiled 27 stations from several campaigns and the observation periods mostly covered one to four years.**” (Lines 178-189)

Although there is mismatch in the temporal coverage between observations and simulation, we mainly focus on the global dust cycle based on multi-year means of both observations and simulations and the impacts on our conclusion due to the mismatch should be not significant. We also add a discussion on the impacts of the inconsistency of data: “**We consider the dataset above as a climatology although some of them did not cover a long enough period such as tens of years. Therefore, for the**

stations with shorter period of observations but large dust variability at interannual to decadal timescales, some model discrepancies may be induced due to the inconsistency between these observations and the model results that are averaged over a period of 45 years. We will discuss this in next sections.” (Lines 202-207) and “The biases may also be partly explained by the consistency between the observations and simulations, especially for those observation which were made at a relatively short-term period (one to several years), as mentioned in Section 3.1.” (Lines 516-518).

**6. Line 220, can you please clarify how dust lifetime is calculated?**

Reply: Dust lifetime is defined as the division of global dust burden (Tg) by total deposition ( $\text{Tg yr}^{-1}$ ) and its unit is changed from years to days. In the revised manuscript, we add an equation (Eq. 8) for the definitions of dust lifetime.

**7. Lines 226-228, only one model year (2000) is used in AeroCom model intercomparisons, while 46-year averages (1960-2005) are used here. This may contribute to the discrepancy as well.**

Reply: We thank the reviewer for the comment. To identify the impacts from different model years, we also compare the CMIP5 model results on year 2000 as AeroCom project. The results show dust emission in year 2000 from CMIP5 models ranges from 773 to 8183  $\text{Tg yr}^{-1}$ , and dust burden in year 2000 ranges from 2.7 to 42 Tg. These ranges are similar to those based on 46-year averages (1960-2005), which are 735-8186  $\text{Tg yr}^{-1}$  and 2.5-41.9 Tg, respectively. Therefore, the difference in model years selected for comparison could only result in slight difference of comparison results and thus can't change our statements and conclusions.

**8. Lines 280-281, “... (Somalia, Ethiopia, and Kenya), East India, and northern part of Indo China Peninsula, which are rarely regarded as potential dust sources”. Nogal Valley of Somalia and the Chalbi desert in Kenya are dust sources (Ginoux et al. 2012).**

Reply: We thank the reviewer for pointing out this. We are sorry our previous statements were not correct. Now in the revised manuscript, we modified our statements by deleting “the Eastern Africa (Somalia, Ethiopia, and Kenya)” and adding the reference of Ginoux et al. (2012).

**9. Lines 291-292, previous studies in addition to “Wu et al. 2018” also identified dust sources in North America, such as Prospero et al. (2002) and Ginoux et al. (2012). Please add more references here.**

Reply: We have added more references as suggested by the reviewer.

**10. Lines 301-302, “The models consistently simulate the largest dust emission in**



***North Africa...”, is this consistent with AeroCom results?***

Reply: Yes. This is consistent with AeroCom results. To clarify, in the revised manuscript, we add a sentence: “**This is consistent with previous model intercomparison of AeroCom (Huneus et al., 2011)**” (Lines 381-382)

***11. Line 340, 0.1 of erodibility?***

Reply: Yes. 0.1 of erodibility is set as a threshold for dust emission occurrence. We have clarified this by changing “a geomorphic source erodibility with a threshold value of 0.1” to “**a geomorphic source erodibility with its threshold of 0.1**” in the revised manuscript.

***12. Line 408, does AOD assimilation affect dust deposition in MERRA2?***

Reply: Yes. AOD assimilation affect dust deposition through impacting dust concentrations in MERRA-2. We have clarified this in Section 3.2: “**The MERRA-2 aerosol reanalysis uses increment analysis update procedure, which derive 3-dimensional analysis increment for aerosol mixing ratio based on the aerosol optical depth (AOD) analysis increment (Randles et al., 2017). The procedure further affects the aerosol deposition flux.**” (Lines 223-226)

***13. Line 418, “classified into two groups”, based on what criteria?***

Reply: We classified the stations into the two groups based on their distance from the dust source regions. The stations in the second group are farther from the dust source regions than the first group. In the revised manuscript, the analysis of fraction of wet deposition is removed due to the relatively short period in observation (please see our reply to minor moment #5).

***14. Line 457, please add “surface” before “dust concentration”***

Reply: Done.

***15. Lines 476-477, the vertical distribution of dust could be another reason. The model may simulate higher dust concentration above the surface.***

Reply: We thank the reviewer for the comment. We agree with the reviewer that the vertical diffusion of dust may be another reason as MIROC5 and MIROC4h differ much in dynamics and physical parameterizations. Therefore, in the revised manuscript, we add a sentence to clarify this: “**Another reason may lie in the vertical diffusion of dust, which also determines the distance of its horizontal transport.**” (Lines 561-562)

**16. Line 496, please add a statistical significance level to correlation coefficients.**

Reply: We add the significant test and the results shows the correlation coefficients are all statistically significant at the 0.005 level. In the revised manuscript, we add a sentence to mention this result: “**All the correlation coefficients are statistically significant at the 0.005 level**” (Lines 581-582)

**Reviewer #2**

***Global dust cycle and uncertainty in CMIP5 models Chenglai Wu, Zhaohui Lin and Xiaohong Liu***

***Presented in this study is an evaluation of the global dust cycle simulated by 15 models participating in the Coupled Model Intercomparison Project (CMIP5). The models are compared with each other, aerosol reanalysis data and station observations of dust deposition and concentration. Differences between model simulated dust emission, load, deposition and other aspects are discussed. I believe this is a very valuable study which allows us to better understand the state of the art of dust modelling and better understand the areas where research is needed.***

***It is probably not surprising that very large differences exist between the model simulated features of the dust cycle, as we already know for some time. It remains a challenge for the models to converge to the truth. This study is a valuable reminder of the challenges ahead and contribution to better quantifying the error bars of the aerosol radiative forcing estimated by climate models.***

***The paper is well written and logically structured, although a more concise description would be my preference.***

***There are a number of issues, which I suggest the authors to consider:***

Reply: We thank Prof. Yaping Shao for his detailed review and encouraging comments. The text, tables, and figures are revised as he suggested.

***Abstract appears to be long.***

Reply: Thank you for the comment. We have shortened our abstract by about 20% in the revised manuscript.

***L11: address their strengths ...***

Reply: We have changed “address the strengths and weaknesses of these models” to “**address their strengths and weaknesses**”.

***L28-29: deposition is a flux, not a sink***

Reply: We thank the reviewer for pointing out this. We have changed “wet deposition is a smaller sink than dry deposition” to “**wet deposition is smaller than dry deposition**”.

***Model data: a description of the dust schemes examined in this study is given in this section. These schemes differ in a number of aspects. It would be helpful if some statements were given here, how it is ensured that the comparison is fair. For instance, all models have the same spatial resolution? Do they use the same land surface data?***

Reply: We thank the reviewer for this good suggestion. The models included here are those models participating in the CMIP5 and used for historical climate change attribution and future climate projection. CMIP5 provides a well-coordinated framework for climate change experiments and the simulations are included in the IPCC AR5. The experiment design in CMIP5 is described in Taylor et al. (2012). Here, we use the historical experiment which cover the period of 1850 to at least 2005. CMIP5 asks the various model groups around the world to run their models with same forcing data including greenhouse and anthropogenic aerosol and precursor emissions, but the groups are allowed to configure the models with their own resolutions and physical parameterizations including dust emission. For dust emission, land surface data is also different as originally set in the models.

In the revised manuscript, we add some statements in Section 2: “**Here we use the historical simulations from 15 CMIP5 models (Table 1). CMIP5 provides a well-coordinated framework for climate change experiments (Taylor et al., 2012). The experiment design in CMIP5 is given in Taylor et al. (2009). The models in CMIP5 were run with their own formulations and resolutions and CMIP5 represented a variety of best-effort attempts to simulate the climate system at the time. CMIP5 results have been included in the Fifth Assessment Report of Intergovernmental Panel on Climate Change (Flato et al., 2013). For the historical experiment, the models were run from 1850 to at least 2005 with same forcing data such as greenhouse gas, solar radiation, and anthropogenic aerosol and precursor emissions (Taylor et al., 2009). All the 15 models used here are fully-coupled models.**” (Lines 96-105) and “**Land cover data are crucial for dust modeling and they also varies in different models. Eleven models use prescribed vegetation or roughness and these data are originated from different studies (an example of this can be seen from the difference between MIROC4h and MIROC5, shown in Section 4.2). In other four models (HadGEM2-CC, HadGEM2-ES, MIROC-ESM, MIROC-ESM-CHEM), dust emission scheme is coupled to dynamic vegetation.**” (Lines 120-125)

***In Section 4.1, I suggest to write explicitly the equation for the global dust budget, and state how the individual terms are computed, so that we can easily understand how the quantities examined are related and why they are chosen. For example, while residence time is important for dust deposition, surface shear stress is***

*important for dust emission, so why is residence time compared here, but not surface shear stress?*

Reply: We thank the reviewer for a good suggestion. We have added several equations to explicitly explain the global dust budget and dust residence time in Section 4.1 (Lines 248-270):

First, we present the global dust budgets in CMIP5 models. The key global budget terms include global dust emission ( $E$ ;  $\text{kg s}^{-1}$ ), dust deposition ( $D$ ;  $\text{kg s}^{-1}$ ), and dust burden ( $B$ ;  $\text{kg}$ ), defined respectively as

$$E = \int F_e dS \quad (1)$$

$$D = \int F_d dS \quad (2)$$

$$B = \int m_b dS \quad (3)$$

where  $F_e$  is emission flux ( $\text{kg m}^{-2} \text{s}^{-1}$ );  $F_d$  is deposition flux ( $\text{kg m}^{-2} \text{s}^{-1}$ );  $m_b$  is column dust concentration ( $\text{kg m}^{-2}$ );  $S$  is surface area ( $\text{m}^2$ ).  $m_b$  is an integration of dust concentration ( $C$ ;  $\text{kg m}^{-3}$ ) over the entire column:

$$m_b = \int C dz \quad (4)$$

The mass equation for dust aerosols around the globe is:

$$\int E dt = \int D dt + \Delta B \quad (5)$$

Or

$$\bar{E} \Delta t = \bar{D} \Delta t + \Delta B \quad (6)$$

where  $\Delta B$  is the change of dust burden between the start time and the end time;  $\bar{E}$  is mean global dust emission;  $\bar{D}$  is mean global dust deposition; and  $\Delta t$  is the cumulative time. For a long-term period,  $\Delta B$  is relatively small (i.e.,  $\Delta B \approx 0$ ), then

$$\bar{E} = \bar{D} \quad (7)$$

Dust deposition can be separated into two terms: dry deposition and wet deposition. According to Eq. (6), the mean dust lifetime (also called residence time;  $\bar{T}$ ) can be defined by assuming  $\bar{E} = 0$  as:

$$\bar{T} = \frac{\bar{B}}{\bar{D}} \quad (8)$$

where  $\bar{B}$  is mean global dust burden.

***L222: may be useful to state, whether we are talking about the same size range. If it is not the same size range, then it is not meaningful to emphasis the range of 735-8196 Tg /a, and a size range correction is necessary. I am not sure whether I missed something, but it is not clear to me whether this is the total emission for the particle size range 0 – 20 microns for all models, or the emission for some models using size range 0 – 20 microns and some 0 – 63 microns.***

Reply: We thank the reviewer for pointing out this. The results in this study are based on all the dust particles included in each model. We have this clarified in Section 2: “as only the total dust emission, deposition, and concentration for the whole size range are provided, we are unable to investigate the difference in the mass partitioning among different dust sizes and its evolution, which will be left for future studies” (Lines 138-140)

We agree with the reviewer that comparison of dust emission results should take into account the different size range. Although we are unable to make all the model results comparable, we classify the models into three groups and the dust size range in each group is identical or similar. Therefore, the global dust emissions in each group are comparable (Table 3). Other results are compared by re-ordering the models (Tables 4-5, Figures 3, 6, 8-9). The difference in the dust size range can be recognized if we compare the results from different groups. Accordingly, the statements in the main text have been revised:

- a. “The results show that the global dust emission in these models ranges by a factor of 4-5 for the same size range” (Abstract, Lines 17-18)
- b. “The dust size ranges considered in the models are not exactly the same. Three models (ACCESS1-0, HadGEM2-CC/ES) consider dust particles with diameter from 0.06 to 63  $\mu\text{m}$ , and estimated global dust emissions range from 2218 to 8186  $\text{Tg yr}^{-1}$ . Seven models (GFDL-CM3, four MIROC models and two MRI models) consider dust particles in the diameter of 0.2-20  $\mu\text{m}$ , and they estimate global dust emission in the range of 735-3598  $\text{Tg yr}^{-1}$ . The remaining five models consider dust particles in diameter below 10-16  $\mu\text{m}$  and they estimate global dust emission of 1677-3698  $\text{Tg}$ . If ACCESS1-0 and HadGEM2-CC/ES are excluded, these estimation here are similar to those of AeroCom models in the similar size range, which gave dust emissions in the range of 514-4313  $\text{Tg yr}^{-1}$  (Huneeus et al., 2011)” (Section 4.1, Lines 274-283)
- c. “Overall, the models with largest dust size ranges (ACCESS1-0, HadGEM2-CC/ES) simulate smaller fraction of wet deposition (12-19 %) than other models (16-39 %).” (Section 4.1, Lines 311-313)
- d. “It is interesting to mention that if ACCESS1-0 with largest dust particle size range (0.06-63  $\mu\text{m}$  in diameter) and largest fraction (91%) for continental deposition is excluded, other six models simulate quite similar fraction of continental deposition (78-83%).” (Section 4.3, Lines 526-529)
- e. “The results show that the global dust emission in these models differs much: from 2218 to 8186  $\text{Tg yr}^{-1}$  (size range of 0.06-63  $\mu\text{m}$  in diameter), from 735 to 3598  $\text{Tg yr}^{-1}$  (size range of 0.06-20  $\mu\text{m}$  in diameter), and from 1677 to 3698  $\text{Tg yr}^{-1}$  (size <16  $\mu\text{m}$  in diameter). The global dust emission ranges by a factor of 4-5 for dust particles in the same size range.” (Section 5, Lines 599-604)

***L245: I recall that in earlier studies dry and wet depositions are about the same order of magnitude, the finding that wet deposition makes only 12-39% of the total deposition is somewhat surprising.***

Reply: We thank the reviewer for the comment. We explore the earlier studies on global dust budget. There are several studies which did show wet deposition was about the same order of magnitude of dry deposition (e.g., Luo et al., 2003). However, there are some studies which showed dry deposition is significantly larger than wet deposition. For example, Ginoux et al. (2004) estimated wet deposition accounts for

10 % of total deposition. In addition, the fourteen AeroCom models estimated the fraction of wet deposition ranges from 16 to 66 %. Therefore, the results of CMIP5 (12-39 %) should lie in the middle to low end of previous estimates. To clarify, we add more discussions on this in the revised manuscript: “Early model studies estimated the fraction of global wet deposition ranges from 10 % (Ginoux et al., 2004) to 49 % (Luo et al., 2003). The 14 AeroCom models estimated the fraction of global wet deposition in the range of 16-66 %. Therefore, this result of 12-39 % lies at the middle to low end of previous estimates.” (Lines 305-308)

*Section 4.2: some dust emission schemes are already adjusted to satellite observed dust load (so much emission is allowed such that the dust load matches the satellite observed global dust load). I think it would be useful to point out which these models are.*

Reply: We thank the reviewer for the suggestion. Six models adopt source erodibility to make the simulated dust patterns close to the observations. We have explicitly mentioned these models in Section 2 (Model data): “In addition, to make the simulated dust patterns close to the observations, the dust schemes in six models (ACCESS1-0, CESM, CSIRO-Mk3-6-0, GFDL-CM3, HaGEM2-CC/ES) further adopt a source erodibility (also called source function) on dust emission. CESM adopts a source erodibility from Zender et al. (2003), and other five models use that of Ginoux et al. (2001).” (Lines 116-120). We also add more discussions in Section 4: “Note CSIRO-Mk3-6.0 and GFDL-CM3, which adopt the same dust emission scheme and source erodibility (Section 2), show similar dust emission regions.” (Lines 447-449).

*Section 5, Discussion and Conclusion: Experience shows that differences in land surface schemes can have a major effect on dust emission estimates, in particular the simulation of soil moisture. It may be useful to say something about it.*

Reply: We thank the reviewer for the comment. Land surface state especially soil moisture is vital for dust emission. The difference in land surface state is involved in the difference in dust emission as well. Following the suggestion, we have added “soil moisture” when discussing “the uncertainty in many aspects of the model” (Lines 667-668). We also add more discussions: “In addition, it is also helpful to setup more constrained experiments to separate the sensitivity of model estimates to individual factors, by varying one single factor such as dust emission scheme (e.g., Wu and Lin, 2013) and land surface scheme (e.g., Lin et al., 2012), or using identical emissions (e.g., Textor et al., 2007)” (Lines 671-675)

*L587-589: Again, is the size issue considered in the comparison? Because mass is proportional to size cubed, a small difference in size range can result in huge differences in the dust budget terms. If size correction is not done, then what we can learn from such an assessment study is limited.*

Reply: We thank the reviewer for the comment. The size issue is not considered fully in the original manuscript, although we have mentioned its impacts. Now in the revised manuscript, we consider carefully the size difference and compared the model results by classifying the models into three groups according to the size ranges (Tables 3). The description in the main text is revised accordingly (see my reply to the comment on L222 above). Here in the Discussions Section, we clarify: “**The results show that the global dust emission in these models differs much: from 2218 to 8186 Tg yr<sup>-1</sup> (size range of 0.06-63 μm in diameter), from 735 to 3598 Tg yr<sup>-1</sup> (size range of 0.06-20 μm in diameter), and from 1677 to 3698 Tg yr<sup>-1</sup> (size <16 μm in diameter). The global dust emission ranges by a factor of 4-5 for dust particles in the same size range.**” (Lines 599-604) and “**We have compared the global dust emission and burden among the models with the same dust size range considered.**” (Lines 693-694)

*I suggest, separate the discussion with conclusion. As it is very a long section.*

Reply: we thank the reviewer for the suggestion. We have separated the previous “5. Discussion and Conclusions” section into two sections: “**5. Conclusions**” and “**6. Future work**”

*Uno et al. (2006 JGR), Textor et al (2006; 2007 ACP) have done model comparisons. These papers may be interesting to this study.*

Reply: We thank the reviewer for pointing out these relevant studies to us. These studies have done great job in quantifying the uncertainties in regional or global dust modeling. Much have learned from these studies. In the revised manuscript, we have cited these references with some discussions (Line 54, Lines 669-670, Line 675).

# 1 Global dust cycle and uncertainty in CMIP5 models

2 Chenglai Wu<sup>1,\*</sup>, Zhaohui Lin<sup>1</sup>, and Xiaohong Liu<sup>2</sup>

3 <sup>1</sup>International Center for Climate and Environment Sciences, Institute of Atmospheric  
4 Physics, Chinese Academy of Sciences, Beijing, China

5 <sup>2</sup>Department of Atmospheric Sciences, Texas A&M University, College Station, USA

6 \* Corresponding author: Chenglai Wu, [wuchenglai@mail.iap.ac.cn](mailto:wuchenglai@mail.iap.ac.cn)

7

## 8 Abstract

9 Dust cycle is an important component of the Earth system and have been  
10 implemented into climate models and Earth System Models (ESMs). An  
11 assessment of the dust cycle in these models is vital to address their strengths and  
12 weaknesses ~~of these models~~ in simulating dust aerosol and its interactions with the  
13 Earth system and enhance the future model developments. This study presents a  
14 comprehensive evaluation of global dust cycle in ~~15-fifteen~~ models participating in  
15 the fifth phase of the Coupled Model Intercomparison Project (CMIP5). The  
16 various models are compared with each other and with an aerosol reanalysis as  
17 well as station observations ~~of dust deposition and concentrations~~. The results  
18 show that the global dust emission in these models ranges ~~from 735 to 8186 Tg yr<sup>-1</sup>~~  
19 ~~\*by a factor of 4-5 for the same size range and the annual mean dust burden ranges~~  
20 ~~from 2.5 to 41.9 Tg, both of which scatter by a factor of about 10-20~~. The models  
21 generally agree with each other and observations in reproducing the “dust belt”  
22 that extends from North Africa, Middle East, Central and South Asia, to East Asia,



23 although they differ largely in the spatial extent of this dust belt. The models also  
24 differ in other dust source regions such as North America and Australia, ~~where the~~  
25 ~~contributions of these sources to global dust emissions vary by a factor of more~~  
26 ~~than 500~~. We suggest that the coupling of dust emission with dynamic vegetation  
27 can enlarge the range of simulated dust emission.

28 For the removal process, all the models estimate that wet deposition is a  
29 smaller ~~sink~~ than dry deposition and wet deposition accounts for 12-39 % of total  
30 deposition. The models also estimate that most (77-91 %) of dust particles are  
31 deposited onto continents and 9-23 % of them are deposited into oceans. ~~A linear~~  
32 ~~relationship between dust burden, lifetime, and fraction of wet deposition to total~~  
33 ~~deposition from these models suggests a general consistency among the models.~~  
34 Compared to the observations, most models reproduce the dust deposition and dust  
35 concentrations within a factor of 10 at most stations, but larger biases by more  
36 than a factor of 10 are also noted at specific regions and for certain models. These  
37 results ~~cast a doubt on the interpretation of the simulations of dust affected fields~~  
38 ~~in climate models and~~ highlight the need for further improvements of dust cycle  
39 especially on dust emission in climate models.

40

41

## 42 1. Introduction

43 Dust cycle is an important component of the Earth system as it has strong impacts  
44 on the Earth environment and climate system (Shao et al., 2011). Dust aerosol in the  
45 atmosphere significantly impacts the climate systems via various pathways, such as  
46 scattering and absorbing the solar and terrestrial radiation, modifying cloud radiative  
47 forcing by acting as cloud condensation nuclei and ice nucleating particles, and reducing  
48 the snow albedo when depositing onto snow (Boucher et al., 2013; Forster et al., 2007;  
49 Liu, et al., 2012a; Mahowald et al., 2011; Wu et al., 2018a; Rahimi et al., 2019). Dust  
50 affects the biogeochemical cycle by delivering the nutrients (e.g., mineral, nitrogen, and  
51 phosphorus) from dust sources to the oceans/other continents (Jickells et al., 2005;  
52 Mahowald et al., 2011). Dust aerosol is also one of the main contributors to air pollution  
53 that is hazardous to human health (Bell et al., 2008; Lin et al., 2012).

54 To quantify the dust impacts on Earth system, dust cycle including dust emission,  
55 transport, and dry and wet deposition has been incorporated in climate models and Earth  
56 System Models (ESMs) since 1990s. These models have the capability to reproduce the  
57 general patterns of global dust distribution (e.g., Ginoux et al., 2001; Zender et al., 2003;  
58 Yue et al., 2009; Huneeus et al., 2011; Liu et al., 2012b). However, large uncertainties  
59 still exist in the simulated global dust budgets in these models, as revealed by a wide  
60 range of model results (e.g., [Textor et al., 2006](#); [Huneeus et al., 2011](#)). A comparison of  
61 14 different models from the Aerosol Comparison between Observations and Models  
62 (AeroCom) Phase I showed the estimated global dust emission ranges from 514 to 4313  
63 Tg yr<sup>-1</sup> and annual mean dust burden from 6.8 to 29.5 Tg (Huneeus et al., 2011).  
64 Compared to the observations, these models from AeroCom Phase I produce the dust

65 deposition and surface concentration mostly within a factor of 10 (Huneeus et al., 2011).  
66 Uncertainties of dust cycle have led to difficulty in the interpretation of climate impacts  
67 of dust aerosol (Yue et al., 2010; Forster et al., 2007; Boucher et al., 2013).

68 The Coupled Model Intercomparison Project Phase 5 (CMIP5) provides a  
69 comprehensive dataset of meteorological variables and climate forcing agents such as  
70 aerosols including dust during the period of 1850s to 2000s from a variety of climate  
71 models and ESMs. Dust cycle is interactively calculated in some CMIP5 models for  
72 historical climate simulations and future climate projections. Till now, only a few studies  
73 have investigated dust simulations in CMIP5. Evan et al. (2014) evaluated African dust in  
74 23 CMIP5 models and found the models underestimate dust emission, deposition, and  
75 aerosol optical depth (AOD) and have low ability in reproducing the interannual  
76 variations of dust burden. Pu and Ginoux (2018) compared the dust optical depth (DOD)  
77 from 7 CMIP5 models with satellite observations from 2004 to 2016. They found that  
78 these models can capture the global spatial patterns of DOD but with an underestimation  
79 of DOD by 25.2% in the boreal spring, and some models cannot capture the seasonal  
80 variations of DOD in several key regions such as Northern China and Australia. Wu et al.  
81 (2018b) evaluated the dust emission in East Asia from 15 CMIP5 models and found that  
82 none of the models can reproduce the observed decline trend of dust event frequency  
83 from 1961 to 2005 over East Asia.

84 None of the above studies has investigated the global dust cycles including their  
85 sources and sinks in the CMIP5 models. Therefore, this study is aimed at filling the gap  
86 by presenting the strengths and weaknesses of CMIP5 models in simulating global dust  
87 cycles. This study will also investigate the associated model uncertainties. As there are a

88 variety of complexities in the CMIP5 models (Flato et al., 2013), this study aims at  
89 identifying the difference in simulated dust cycle as a result of these different  
90 complexities. Of particular interest is that some models couple dust emission with  
91 dynamic vegetation while the others calculate dust emission based on prescribed  
92 vegetation conditions (Table 1), and thus the impacts of dynamic vegetation on dust  
93 emission can be examined by comparing the results from these two ~~group types of~~  
94 models, which has been rarely studied previously.

95 The paper is organized as follows. Section 2 introduces the CMIP5 models,  
96 including the dust emission parameterization. Section 3 describes the observation data  
97 used for model validation. Section 4 presents the global dust budget and dust emission,  
98 followed by evaluations of dust deposition flux and dust concentration with observations.  
99 Discussion and conclusions are given in section 5.

100

## 101 2. Model data

102 Here we use the historical simulations from 15 CMIP5 models (Table 1). CMIP5  
103 provides a well-coordinated framework for climate change experiments (Taylor et al.,  
104 2012). The experiment design in CMIP5 is given in Taylor et al. (2009). The models in  
105 CMIP5 were run with their own formulations and resolutions and CMIP5 represented a  
106 variety of best-effort attempts to simulate the climate system at the time. CMIP5 results  
107 have been included in the Fifth Assessment Report of Intergovernmental Panel on  
108 Climate Change (Flato et al., 2013). For the historical experiment, the models were run  
109 from 1850 to at least 2005 with same forcing data such as greenhouse gas, solar radiation,  
110 and anthropogenic aerosol and precursor emissions (Taylor et al., 2009). All the 15

111 models used here are fully-coupled models ~~used for historical climate simulations and~~  
112 ~~future climate projections, which are included in the Fifth Assessment Report of~~  
113 ~~Intergovernmental Panel on Climate Change (Flato et al., 2013)~~. A brief description of  
114 these model is given in Table 1 and more detailed information can be found in the  
115 references as listed.

116 An essential part of dust cycle is dust emission. The dust emission schemes used in  
117 these models and the references are also listed in Table 1. Here we only provide a brief  
118 summary of similarities and differences in these dust emission schemes. More details can  
119 be found in the references (Cakmur et al., 2006; Ginoux et al., 2001, 2004; Marticorena  
120 & Bergametti, 1995; Miller et al., 2006; Shao et al., 1996; Takemura et al., 2000, 2009;  
121 Tanaka & Chiba, 2005, 2006; Woodward, 2001, 2011; Zender et al., 2003). In general,  
122 these emission schemes similarly calculate dust emission based on near-surface wind  
123 velocity (in terms of friction wind velocity or wind velocity at 10 m), soil wetness and  
124 vegetation cover, and they mainly differ in how to account for these factors and  
125 associated input parameters. In addition, to make the simulated dust patterns close to the  
126 observations, the dust schemes in six models (ACCESS1-0, HadGEM2-CC/ES, GFDL-  
127 CM3, CESM1-CAM5, CSIRO-Mk3-6-0) further adopt a source erodibility (also called  
128 source function) on dust emission. CESM1-CAM5 adopts a source erodibility from  
129 Zender et al. (2003), and other five models use that of Ginoux et al. (2001). Particularly,  
130 Land cover data are crucial for dust modeling and they also varies in different models.  
131 Eleven models use prescribed vegetation or roughness and these data are originated from  
132 different studies (an example of this can be seen from the difference between MIROC4h  
133 and MIROC5, shown in Section 4.2). In other four models (HadGEM2-CC, HadGEM2-

134 [ES, MIROC-ESM, MIROC-ESM-CHEM](#)), dust emission scheme is coupled to dynamic  
135 vegetation ~~in 5 models (GFDL-CM3, HadGEM2-CC, HadGEM2-ES, MIROC-ESM,~~  
136 ~~MIROC-ESM-CHEM)~~. These models use prognostic vegetation to determine the dust  
137 source regions. This introduces additional degrees of freedom and thus increases the  
138 difficulty in simulating dust emission in these models compared to other models with  
139 prescribed vegetation that is constructed from the observation. This will be discussed in  
140 Section 4.

141 Another difference in dust emission scheme is the treatment of dust sizes including  
142 the size range and mass partitioning in different sizes. 7 models (GFDL-CM3, MIROC4h,  
143 MIROC5, MIROC-ESM, MIROC-ESM-CHEM, MRI-CGCM3, MRI-ESM1) have the  
144 same dust size range of 0.2-20  $\mu\text{m}$  in diameter. 5 of the other eight models (CanESM2,  
145 CESM1-CAM5, CSIRO-Mk3-6-0, GISS-E2-H, GISS-E2-R) have smaller size ranges  
146 (listed in Table 1), while the remaining 3 models (ACCESS1-0, HadGEM2-CC,  
147 HadGEM2-ES) have the larger size range of 0.0632-63.2  $\mu\text{m}$  [in diameter](#). The impacts of  
148 dust size distribution on the simulation of dust cycle will be discussed in later sections.

149 However, as only the total dust emission, deposition, and concentration [for the whole size](#)  
150 [range](#) are provided, we are unable to investigate the difference in the mass partitioning  
151 among different dust sizes and its evolution, which will be left for future studies.

152 Note that we select these models because they calculate dust emission interactively  
153 by their dust emission schemes implemented, and meanwhile, model output of dust  
154 emission flux and dust concentration are available from the CMIP5 archive. [These](#)  
155 [models have different horizontal resolutions \(Table 1\). To generate multi-model statistics](#)  
156 [of dust emission intensity \(Section 4.2\), individual model results are interpolated to the](#)

157 [coarsest resolution among these models \(i.e., 2.8° × 2.8°\) using area conserve remapping](#)  
158  [\(http://www.ncl.ucar.edu/Document/Functions/Contributed/area\\_conserve\\_remap\\_Wrap.](http://www.ncl.ucar.edu/Document/Functions/Contributed/area_conserve_remap_Wrap.shtml)  
159 [shtml, accessed on 6 June 2020\).](#)

160 Also note that not all the models have both dry and wet deposition archived and 8  
161 models provide only dry (GFDL-CM3) or wet deposition flux ([HadGEM2-CC,](#)  
162 [HadGEM2-ES](#)~~CSIRO-Mk3-6-0, HadGEM2-CC, HadGEM2-ES,~~ MIROC4h, MIROC5,  
163 MIROC-ESM, MIROC-ESM-CHEM, [CSIRO-Mk3-6-0](#)). Therefore, for dust deposition,  
164 we derive the global total amount of dry (wet) deposition by subtracting wet (dry)  
165 deposition from emission if only wet (dry) deposition is available. For comparison with  
166 station observations, we will only use seven models with both dry and wet deposition  
167 provided. If there are multiple ensemble simulations available for a specific model, we  
168 will use the ensemble means from these simulations for this model (Table 1). The  
169 historical simulations of CMIP5 cover the period of 1850-2005. However, some model  
170 results prior to 1960 or 1950 are not provided in the CMIP5 archive (e.g., ensemble #2  
171 and #3 from HadGEM2-CC prior to 1960 is not available; MIROC4h prior to 1950 is not  
172 available). Therefore, we will focus on the period of 1960-2005 to include as many  
173 models as possible and to include as many years as possible for the analysis of present-  
174 day dust cycle.

175 ~~To evaluate the CMIP5 model results, we also use the Modern Era Retrospective~~  
176 ~~Analysis for Research and Applications, version 2 (MERRA 2). MERRA 2 is the latest~~  
177 ~~atmospheric reanalysis produced by NASA's Global Modeling and Assimilation Office~~  
178 ~~(Gelaro et al., 2017). MERRA 2 assimilates more observation types and have improved~~  
179 ~~significantly compared to its processor, MERRA. A major advancement of MERRA 2 is~~

180 ~~that it includes the assimilation of AOD (Randles et al., 2017), which is not included in~~  
181 ~~MERRA and other commonly used reanalysis datasets such as ECWMF Reanalysis~~  
182 ~~(ERA5) and NCEP/DOE Reanalysis II (R2). The aerosol fields (including dust) in~~  
183 ~~MERRA 2 are significantly improved compared to an identical control simulation that~~  
184 ~~does not include the AOD assimilation (Randles et al., 2017; Buchard et al., 2017). It~~  
185 ~~should be noted that as only AOD is taken into account in the aerosol assimilation, there~~  
186 ~~may be discrepancies in the related aerosol fields such as aerosol concentration and~~  
187 ~~deposition. In addition, dust emission is calculated directly from surface wind speed and~~  
188 ~~soil wetness based on the dust emission scheme of Ginoux et al. (2001), and there is no~~  
189 ~~direct impact on emission from aerosol assimilation. Therefore, there may be~~  
190 ~~inconsistence between dust emission, burden, and deposition. In fact, as shown in the~~  
191 ~~Section 4, there is imbalance between total dust emission and deposition globally and~~  
192 ~~adjustment of dust emission to fit the dust burden is still needed. Despite the limitation,~~  
193 ~~MERRA 2 provides a well-constrained global dust dataset, which is very useful for~~  
194 ~~model evaluations. We will use MERRA 2 as a referential data but with the knowledge~~  
195 ~~of its limitation. We will use the long-term means of dust-related variables during the~~  
196 ~~whole period when data is available (i.e., 1980–2018). Dust in MERRA 2 is treated by~~  
197 ~~five size bins spanning from 0.2 to 20  $\mu\text{m}$ , which are summed to provide the total values.~~  
198 ~~MERRA 2 is provided at the resolution of  $0.5^\circ \times 0.625^\circ$ , which is similar to one CMIP5~~  
199 ~~model (MIROC4h) and finer than other CMIP5 models.~~

200

### 201 **3. Observations**Reference data

#### 202 **3.1. Observations**

设置了格式: 字体: 加粗

带格式的: 列表段落, 首行缩进: 0 字符, 多级符号 + 级别: 2 + 编号样式: 1, 2, 3, ... + 起始编号: 1 + 对齐方式: 左侧 + 对齐位置: 0 厘米 + 缩进位置: 0.71 厘米



203           There are limited observational datasets that can be used for model evaluations.  
204   There is no direct observation of dust emission flux, but satellite observations can provide  
205   the locations of dust source regions where dust appears most frequently (e.g., Prospero et  
206   al., 2002; Ginoux et al., 2012). Here we do not directly use these observations as they are  
207   not available for our usage, but we will refer to the dust source map based on satellite  
208   observations from previous studies (e.g., Prospero et al., 2002; Ginoux et al., 2012) and  
209   qualitatively compare simulated dust emission regions with them.

210           Dust deposition is an important constraint on the global dust budget. Here we use  
211   the dust deposition flux at 84 stations across the globe available from the AeroCom  
212   project (Huneeus et al., 2011). The dataset is compiled from the Dust Indicators and  
213   Records in Terrestrial and Marine Paleoenvironments (DIRTMAP) database (Kohfeld  
214   and Harrison, 2001; [Tegen et al., 2002](#)) and the data of Ginoux et al., (2001) and  
215   Mahowald et al. (1999, 2009). [The observation periods varied for different stations. Dust  
216   deposition from DIRTMAP is from sediment traps and following Tegen et al. \(2002\), we  
217   only use those 41 stations with deployment period larger than 50 days. Original data of  
218   Ginoux et al. \(2001\) contains both measurements and model estimates. We only use the  
219   measurements from Ginoux et al. \(2001\) which consists of 10 stations and the  
220   observation periods varied from 1 to 20 years \(see sites # 2, 3, 4, 5, 6, 7, 8, 14, 15, 16 in  
221   Table 6 of Ginoux et al. \(2001\)\). Data of Mahowald et al. \(1999\) was derived from ice  
222   core data and consists of 6 stations. Except at one of station \(i.e., Renland\) where the  
223   period was 5 years \(i.e., 1813-1819 excluding 1816-1817\), the exact observation periods  
224   at other 5 stations were not provided and generally covered a time slice of tens of years or  
225   more for current climate. In addition, Mahowald et al. \(2009\) further compiled 27 stations](#)

226 ~~from several campaigns and the observation periods mostly covered one to four years.~~  
227 ~~Dust deposition flux are recorded over a period of several to hundreds of years at these~~  
228 ~~stations. There are two types of deposition, dry deposition and wet deposition. To~~  
229 ~~evaluate the contribution of wet deposition to total deposition, we also use the fraction of~~  
230 ~~wet deposition to total deposition at 10 stations, which is compiled by Mahowald et al.~~  
231 ~~(2011). The fraction of wet deposition is obtained from the observations over several~~  
232 ~~years. Note as only minimum and maximum values of fraction of wet deposition are~~  
233 ~~provided for some stations, the average of the minimum and maximum values will be~~  
234 ~~plotted with the range provided when compared with the simulations.~~

235 Dust concentration is a key variable that reflects both the dust emission and  
236 transport. We use the monthly surface dust concentrations at 20 sites managed by the  
237 Rosenstiel School of Marine and Atmospheric Science at the University of Miami  
238 (Prospero, 1996). We also use the monthly surface dust concentrations measured at 2  
239 other stations: Rukomechi, Zimbabwe (Maenhaut et al., 2000a; Nyanganyura et al., 2007)  
240 and Jabiru, Australia (Maenhaut et al., 2000b; Vanderzalm et al., 2003). In total, there are  
241 22 stations globally. These stations are generally located in the downwind of dust source  
242 regions and some of them are located in the remote regions (Table 2; Figure 1).

243 Measurements at these stations are taken over a period of two to tens of years (Table 2).  
244 This dataset has been widely used to evaluate global dust models (e.g., Ginoux et al.,  
245 2001; Zender et al., 2003; Liu et al., 2012b) and also included in the AeroCom project  
246 (Huneus et al., 2011).

247 We consider the dataset above as a climatology although some of them did not cover  
248 a long enough period such as tens of years. Therefore, for the stations with shorter period

249 of observations but large dust variability at interannual to decadal timescales, some  
250 model discrepancies may be induced due to the inconsistency between these observations  
251 and the model results that are averaged over a period of 45 years. We will discuss this in  
252 next sections. The distribution of these stations (for dust deposition, fraction of wet  
253 deposition, surface dust concentration) are shown in Figure 1. To compare model results  
254 with station observations, bi-linear interpolation is used to generate the model results at  
255 the stations.

### 257 3.2 MERRA-2 reanalysis

258 Because the station observations are limited in space coverage (Figure 1). To  
259 evaluate the CMIP5 model results, we also use the aerosol reanalysis from Modern-Era  
260 Retrospective Analysis for Research and Applications, version 2 (MERRA-2) to evaluate  
261 the CMIP5 model results. MERRA-2 is the latest atmospheric reanalysis produced by  
262 NASA's Global Modeling and Assimilation Office (Gelaro et al., 2017). MERRA-2  
263 assimilates more observation types and have improved significantly compared to its  
264 processor, MERRA. A major advancement of MERRA-2 is that it includes the  
265 assimilation of AOD (Randles et al., 2017), which is not included in MERRA and other  
266 commonly used reanalysis datasets such as ECWMF Reanalysis (ERA5) and  
267 NCEP/DOE Reanalysis II (R2). The aerosol fields (including dust) in MERRA-2 are  
268 significantly improved compared to an identical control simulation that does not include  
269 the AOD assimilation (Randles et al., 2017; Buchard et al., 2017).

270 The MERRA-2 aerosol reanalysis uses increment analysis update procedure, which  
271 derives 3-dimensional analysis increment for aerosol mixing ratio based on the aerosol

设置了格式: 字体: 加粗

带格式的: 列表段落, 首行缩进: 0 字符, 多级符号 +  
级别: 2 + 编号样式: 1, 2, 3, ... + 起始编号: 1 + 对  
齐方式: 左侧 + 对齐位置: 0 厘米 + 缩进位置: 0.71  
厘米

272 optical depth (AOD) analysis increment (Randles et al., 2017). The procedure further  
273 affects the aerosol deposition flux. It should be noted that as only AOD is taken into  
274 account in the aerosol assimilation, there may be discrepancies in the individual related  
275 aerosol fields components including such as dust aerosol concentration and deposition if the  
276 underlying aerosol model has a bias in one aerosol component. This will also cause  
277 discrepancies in aerosol deposition flux that depends on the aerosol concentration and  
278 deposition velocity. In addition, dust emission is calculated directly from surface wind  
279 speed and soil wetness based on the dust emission scheme of Ginoux et al. (2001), and  
280 there is no direct impact on emission from aerosol assimilation. Therefore, there may be  
281 inconsistence between dust emission, burden, and deposition. In fact, as shown in the  
282 Section 4, there is imbalance between total dust emission and deposition globally and  
283 adjustment of dust emission to fit the dust burden is still needed.

284 Despite the aforementioned limitations, MERRA-2 provides a well-constrained  
285 global dust dataset, which is very useful for model evaluations. We will use MERRA-2 as  
286 a referential data but with the knowledge of its limitation. We will use the long-term  
287 means of dust-related variables during the whole period when data is available (i.e.,  
288 1980-2018). Dust in MERRA-2 is treated by five size bins spanning from 0.2 to 20  $\mu\text{m}$ ,  
289 which are summed to provide the total values. MERRA-2 is provided at the resolution of  
290 0.5°×0.625°, which is similar to one CMIP5 model (MIROC4h) and finer than other  
291 CMIP5 models.

292  
293

#### 294 **4. Results**

带格式的：缩进：首行缩进： 0.85 厘米，定义网格后不调整右缩进，无孤行控制，不调整西文与中文之间的空格，不调整中文和数字之间的空格

#### 295 4.1 Global dust budget

296 First, we present the global dust budgets in CMIP5 models. The key global budget  
297 terms include global dust emission ( $E$ ;  $\text{kg s}^{-1}$ ), dust deposition ( $D$ ;  $\text{kg s}^{-1}$ ), and dust burden  
298 ( $B$ ;  $\text{kg}$ ), defined respectively as

$$299 E = \int F_e dS \text{ (1)}$$

$$300 D = \int F_d dS \text{ (2)}$$

$$301 B = \int m_b dS \text{ (3)}$$

302 where  $F_e$  is emission flux ( $\text{kg m}^{-2} \text{s}^{-1}$ );  $F_d$  is deposition flux ( $\text{kg m}^{-2} \text{s}^{-1}$ );  $m_b$  is column dust  
303 concentration ( $\text{kg m}^{-2}$ );  $S$  is surface area ( $\text{m}^2$ ).  $m_b$  is an integration of dust concentration  
304 ( $C$ ;  $\text{kg m}^{-3}$ ) over the entire column:

$$305 m_b = \int C dz \text{ (4)}$$

306 The mass equation for dust aerosols around the globe is:

$$307 \int E dt = \int D dt + \Delta B \text{ (5)}$$

308 Or

$$309 \bar{E} \Delta t = \bar{D} \Delta t + \Delta B \text{ (6)}$$

310 where  $\Delta B$  is the change of dust burden between the start time and the end time;  $\bar{E}$  is mean  
311 global dust emission;  $\bar{D}$  is mean global dust deposition; and  $\Delta t$  is the cumulative time. For  
312 a long-term period,  $\Delta B$  is relatively small (i.e.,  $\Delta B \approx 0$ ), then

$$313 \bar{E} = \bar{D} \text{ (7)}$$

314 Dust deposition can be separated into two terms: dry deposition and wet deposition.

315 According to Eq. (6), the mean dust lifetime (also called residence time;  $\bar{T}$ ) can be  
316 defined by assuming  $\bar{E} = 0$  as:

317

318

$$\bar{T} = \frac{\bar{B}}{D} \quad (8)$$

319 where  $\bar{B}$  is mean global dust burden.

带格式的: 缩进: 首行缩进: 0 字符

320 Table 3 lists the global dust emission, wet deposition, burden, and lifetime in all the

321 15 models. Global dust emission and wet deposition is given in Tg yr<sup>-1</sup>; burden is given

设置了格式: 上标

322 in Tg; lifetime is given in days. The area fraction of global dust emissions and ratio of

323 wet deposition to total deposition are also given. The dust size ranges considered in the

324 models are not exactly the same. Three models (ACCESS1-0, HadGEM2-CC/ES)

325 consider dust particles with diameter from 0.06 to 63  $\mu\text{m}$ , and estimated global dust

326 emissions range from 2218 to 8186 Tg yr<sup>-1</sup>. Seven models (GFDL-CM3, four MIROC

327 models and two MRI models) consider dust particles in the diameter of 0.2-20  $\mu\text{m}$ , and

328 they estimate global dust emission in the range of 735-3598 Tg yr<sup>-1</sup>. The remaining five

329 models consider dust particles in diameter below 10-16  $\mu\text{m}$  and they estimate global dust

330 emission of 1677-3698 Tg. If ACCESS1-0 and HadGEM2-CC/ES are excluded, these

331 estimation here are similar to Overall, the models estimate the global dust emission in the

332 range of 735-8196 Tg yr<sup>-1</sup>, with the MIROC4h having the lowest and two Hadley models

333 (HadGEM2-CC and HadGEM2-ES) having the highest emissions. The global dust

334 emissions in CMIP5 models differ by about 11 times compared to about 8 times in the

335 those of AeroCom models in the similar size range, which gave dust emissions in the

336 range of 514-4313 Tg yr<sup>-1</sup> (Huneeus et al., 2011). This can be ascribed to a larger

337 difference in the complexity of CMIP5 models compared to AeroCom models (Section 2).

338 In particular, HadGEM2-CC and HadGEM2-ES give more than about twice of the

339 largest emission estimated in the AeroCom models other CMIP5 model estimates. The

340 larger value in HadGEM2-CC and HadGEM2-ES is mainly due to the larger dust size

341 range in the models (0.06 to 63  $\mu\text{m}$ ). Indeed, they simulate 3300 Tg yr<sup>-1</sup> of dust emission  
342 for particles smaller than 20  $\mu\text{m}$  diameter (Bellouin et al., 2011), which falls between the  
343 range of other estimations. ~~the overestimation of bare soil area by the dynamic vegetation~~  
344 ~~module in these models (Collins et al., 2011; Martin et al., 2011).~~ Additionally, the larger  
345 value may be also related to the larger dust size range in the models (0.06 to 63  $\mu\text{m}$ ) with  
346 about 3300 Tg yr<sup>-1</sup> of dust emission for particles smaller than 20  $\mu\text{m}$  diameter (Bellouin  
347 et al., 2011). However, ACCESS1.0 with the same size range as HadGEM2-CC and  
348 HadGEM2-ES produces 3-4 times smaller dust mission. As shown in the evaluation of  
349 surface dust concentrations in Section 4.4, HadGEM2-CC and HadGEM2-ES simulate  
350 well the surface dust concentrations downwind of North Africa and East Asia, but largely  
351 consistently overestimate the surface dust concentrations at the selected stations in other  
352 regions (by more than 5 times on average). This overestimation is related to the  
353 overestimation of excessive bare soil area simulated by the dynamic vegetation module in  
354 these models (Collins et al., 2011; Martin et al., 2011), as will be shown in Section 4.2.  
355 MIROC4h has the smallest global dust emission (735 Tg yr<sup>-1</sup>), which is also much  
356 smaller than other estimates (1246-3598 Tg yr<sup>-1</sup>) in the same size range (0.2-20  $\mu\text{m}$  in  
357 diameter). MIROC4h estimate may be too low, as t~~he~~ MIROC4h model underestimates  
358 the surface dust concentrations by more than 10 times (Section 4.4). If the estimations of  
359 MIROC4h, HadGEM2-CC, and HadGEM2-ES, MIROC4h are not considered, global  
360 dust emissions in CMIP5 models are in the range of 1246-3698 Tg yr<sup>-1</sup>, comparable to  
361 AeroCom results (Huneeus et al., 2011) and other estimations (e.g., Shao et al., 2011).  
362 The global dust emission in MERRA-2 is 1620 Tg yr<sup>-1</sup>, which is within the range of  
363 CMIP5 models.

设置了格式: 非上标/ 下标

364 For dust deposition, dust particles are deposited to the Earth's surface mainly by dry  
365 deposition, and wet deposition accounts for 12-39% of total deposition in CMIP5 models.  
366 Early model studies estimated the fraction of global wet deposition ranges from 10 %  
367 (Ginoux et al., 2004) to 49 % (Luo et al., 2003). The 14 AeroCom models estimated the  
368 fraction of global wet deposition in the range of 16-66 %. Therefore, this result of 12-39 %  
369 lies at the middle to low end of previous estimates. The ratio of wet deposition to total  
370 deposition depends on several factors, for example, dust size distribution, geographical  
371 locations of dust emission regions, and climate states such as circulation and precipitation  
372 (e.g., Wu and Lin, 2013). Overall, the models with largest dust size ranges (ACCESS1-0,  
373 HadGEM2-CC/ES) simulate smaller fraction of wet deposition (12-19 %) than other  
374 models (16-39 %). The estimated global dust burden ranges from 2.5 to 41.9 Tg, and  
375 from 8.1 to 36.1 Tg when ~~MIROC4h~~ and HadGEM2-CC/ES and MIROC4h are excluded.  
376 The lifetime of global dust particles ranges from 1.3 to 4.4 days. The dust burden  
377 (lifetime) in MERRA-2 is 20.3 Tg (4.1 days), which is larger (longer) than most CMIP5  
378 models. The fraction of wet deposition to total deposition in MERRA-2 is 38.6%, which  
379 is in the upper end of CMIP5 results. There is a linear relationship (with the correlation  
380 coefficient  $R=0.67$ , above the statistically significant level of 0.01) between global dust  
381 burden and lifetime in CMIP5 models (excluding HadGEM2-CC/ES; Figure 2a),  
382 indicating a longer lifetime of dust is generally associated with a larger dust burden.  
383 Linear relationship ( $R=0.46$ , above the statistically significant level of 0.05) is also found  
384 between lifetime and fraction of wet deposition (Figure 2b), which indicates that a longer  
385 lifetime corresponds to a larger fraction of wet deposition in the total deposition.  
386



387 **4.2 Global dust emissions**

388 **4.2.1 Spatial distributions**

389 Dust emission is the first and the foremost process in the dust cycle and determines  
390 the amount of dust entrained into the atmosphere. Figure 3 shows the spatial distribution  
391 of dust emission fluxes from 15 CMIP5 models and MERRA-2 reanalysis. In general, all  
392 the models can reproduce the main dust sources, known as the “dust belt” that extends  
393 from North Africa, Middle East, Central Asia, South Asia, to East Asia and that can be  
394 seen from satellite observations (Prospero et al., 2002; Ginoux et al., 2012). This result is  
395 consistent with Pu and Ginoux (2018) that investigated the global distribution of dust  
396 optical depth in seven CMIP5 models. However, the models differ significantly in the  
397 extent of this “dust belt”. Although a large group of CMIP5 models (~~CSIRO-Mk3-6-0,~~  
398 ~~GFDL-CM3,~~ ~~GISS-E2-H/S,~~ MIROC5, MIROC-ESM, MIROC-ESM-CHEM, MRI-  
399 CGCM3, ~~and~~ MRI-ESM1, CSIRO-Mk3-6-0, GISS-E2-H/S) simulate similarly the dust  
400 emission regions mostly over deserts and adjacent arid/semi-arid regions, two of the  
401 models (~~CESM1-CAM5 and~~ MIROC4h and CESM1-CAM5 ~~MIROC4h~~) simulate much  
402 smaller areas of dust emission and a few others (ACCESS1-0, ~~CanESM2,~~ HadGEM2-  
403 CC/ES, CanESM2) simulate more extended dust emission regions. CESM1-CAM5  
404 simulates isolated dust emission regions with “hot spots” of dust emissions larger than  
405 500 g m<sup>-2</sup> yr<sup>-1</sup>, and dust emission in MIROC4h concentrates only over the centers of  
406 deserts. In contrast, ACCESS1-0, ~~CanESM2, and~~ HadGEM2-CC/ES, and CanESM2 not  
407 only simulate the dust emissions in deserts and adjacent regions, but also produce a  
408 considerable amount of dust emissions over the ~~Eastern Africa (Somalia, Ethiopia, and~~  
409 ~~Kenya),~~ East India, and northern part of Indo China Peninsula, which are rarely regarded

设置了格式: 字体: 加粗  
带格式的: 列表段落, 缩进: 左侧: 0 厘米, 首行缩进:  
0 字符, 多级符号 + 级别: 3 + 编号样式: 1, 2, 3,  
... + 起始编号: 1 + 对齐方式: 左侧 + 对齐位置: 1.5  
厘米 + 缩进位置: 2.5 厘米

410 as potential dust sources ([Shao, 2008](#); Formenti et al., 2011; ~~Shao, 2008~~ [Ginoux et al.,](#)  
411 [2012](#)). The extent of “dust belt” can be more clearly seen when we zoom in specific  
412 [regions such as North Africa \(Evan et al., 2014\) and East Asia \(Wu et al., 2018b\)](#). For  
413 [example, in East Asia, although the CMIP5 models can reproduce the dust emissions in](#)  
414 [the deserts of northern China and southern Mongolia, they differ greatly in the edges of](#)  
415 [these deserts, with three models \(MIROC5, CanESM2, and CSIRO-MK3-6-0\) simulating](#)  
416 [dust emission over Tibetan Plateau and seven models \(e.g., ACCESS1-0\) simulating dust](#)  
417 [emission in the southern part of North China \(Wu et al., 2018b\)](#).

418 Dust sources also exist in Australia, North America, South America, and South  
419 Africa, as evident from surface observations (e.g., Shao, 2008) and satellite observations  
420 (Prospero et al., 2002; Ginoux et al., 2012), although the emission fluxes are smaller than  
421 those in the aforementioned “dust belt”. In these regions, most models produce a  
422 considerable amount of dust emissions ( $>5 \text{ g m}^{-2} \text{ yr}^{-1}$ ), while a small group of models  
423 simulate much less or even negligible dust emissions. The models differ greatly in these  
424 regions. For example, in Australia, two models (MIROC-ESM and MIROC-ESM-CHEM)  
425 produces little dust emissions, while seven models (ACCESS1-0, [HadGEM2-CC/ES](#),  
426 [CanESM2](#), CSIRO-Mk3-6-0, GISS-E2-H/R, ~~HadGEM2-CC/ES~~) produce much larger  
427 dust emissions with emission fluxes higher than  $10 \text{ g m}^{-2} \text{ yr}^{-1}$  in a large part of the region.  
428 In North America which also has some dust sources ([Prospero et al., 2002](#); [Ginoux et al.,](#)  
429 [2012](#); Wu et al., 2018a), five models (MIROC4h, MIROC-ESM, MIROC-ESM-CHEM,  
430 MRI-CGCM3, MRI-ESM1) simulate little dust emissions, while four models  
431 (ACCESS1-0, ~~CanESM2~~, HadGEM2-CC/ES, [CanESM2](#)) simulate dust emission fluxes  
432 exceeding  $5 \text{ g m}^{-2} \text{ yr}^{-1}$  in a large part of the region. Note that ACCESS1-0 and ~~CanESM2~~

433 also produce dust emissions in the high latitudes of Northern Hemisphere (>60 °N) and  
434 eastern part of South America. The importance of high latitude dust is recognized  
435 recently (Bullard et al., 2016), but the eastern part of South America has not been  
436 regarded as a potential dust source (Formenti et al., 2011; Shao, 2008).

437

#### 438 4.2.2 Contributions from nine sources

439 The contributions of dust emissions in nine different regions to global dust emission  
440 is summarized in Table 4. The total amount of dust emission in North Africa and East  
441 Asia have been presented in Evan et al. (2014) and Wu et al. (2018b), respectively. Here  
442 we show the results for all the nine regions in the globe and their comparison. The  
443 models consistently simulate the largest dust emission in North Africa, which accounts  
444 for 36-79% of the global total dust emission. This is consistent with previous model  
445 intercomparison of AeroCom (Huneeus et al., 2011). The models also estimate large dust  
446 emissions in Middle East and East Asia, which account for 7-20% and 4-19% of global  
447 dust emission, respectively. The contributions from Central Asia and South Asia in  
448 CMIP5 models range from 1-14% and 0.9-10%, respectively. The contributions from  
449 other sources (North America, South Africa, Australia, South America) are much less  
450 consistent among the models, and the largest difference is in North America (0.008-4.5%)  
451 and Australia (0.02-28%) by three orders of magnitude. The large scatter of CMIP5  
452 results in North America and Australia is also indicated by dust optical depth, as shown  
453 in Pu and Ginoux (2018).

454 Particularly, HadGEM2-CC/ES simulate 25-28% of global dust emission from  
455 Australia, which is comparable to that from sum of all Asian sources (Middle East,

设置了格式: 字体: 加粗  
带格式的: 列表段落, 缩进: 左侧: 0 厘米, 首行缩进:  
0 字符, 多级符号 + 级别: 3 + 编号样式: 1, 2, 3,  
... + 起始编号: 1 + 对齐方式: 左侧 + 对齐位置: 1.5  
厘米 + 缩进位置: 2.5 厘米

456 Central Asia, South Asia, and East Asia). This estimate is unrealistically high, as will be  
457 indicated by the comparison of surface dust concentrations in Section 4.4. The excessive  
458 dust emission in Australia from HadGEM2-CC/ES is mainly ascribed to the excessive  
459 bare soil fraction simulated by HadGEM2-CC/ES, as indicated by its comparison with  
460 International Geosphere-Biosphere Programme (IGBP) data used in ACCESS1-0 (Figure  
461 4a-4c). The overestimation of bare soil fraction in HadGEM2-ES is also illustrated in  
462 Collins et al. (2011). In fact, ~~may be related to the prognostic vegetation used for dust~~  
463 emission, as the ACCESS1-0 model that uses the similar dust emission parameterization  
464 but with the prescribed vegetation from IGBP simulates a much lower dust emission than  
465 HadGEM2-CC/ES. Compared to ACCESS1.0, HadGEM2-CC/ES simulate larger surface  
466 wind speed and slightly smaller soil moisture in Australia (Figures 4d-4i), which can also  
467 partly explain the larger dust emission in HadGEM2-CC/ES.

468 The lowest dust emission in Australia is simulated by MIROC-ESM and MIROC-  
469 ESM-CHEM, which contribute only 0.02-0.03% ( $1 \text{ Tg yr}^{-1}$  or less) to the total dust  
470 emission. This estimate is unrealistically low as Australia is an important dust source  
471 (e.g., Shao et al., 2007) and is also much smaller than previous studies (e.g., Huneeus et  
472 al., 2011). The low dust emission in Australia from MIROC-ESM and MIROC-ESM-  
473 CHEM is related to ~~may be related to~~ the prognostic vegetation used for dust emission. As  
474 shown in Figure 5a-5d, MIROC-ESM and MIROC-ESM-CHEM simulate much larger  
475 leaf area index compared to, ~~as~~ the two other MIROC family models (MIROC4h and  
476 MIROC5). With smaller leaf area index, MIROC4h and MIROC5 simulate significantly  
477 higher dust emissions (~1% of total dust emission).

478 The contributions from nine source regions in MERRA-2 to the total dust emission  
479 are within the range of CMIP5 models. MERRA-2 estimates are obtained through the  
480 assimilation of meteorology in model integrations and therefore uncertainties are reduced.  
481

### 482 4.2.3 Normalized dust emission flux

483 Since the amount of global dust emission differs substantially among different  
484 models, the dust emission flux is further normalized by its global mean value in each  
485 model for the comparison of dust emission area and intensity (Figure 46). Here the dust  
486 emission area is defined as the region with normalized emission flux greater than 0.01. In  
487 Figure 6, we also present the maximum normalized dust emission flux to illustrate the  
488 spatial heterogeneity. -Among the CMIP5 models, MIROC4h ~~CESM-CAM5~~ and CESM-  
489 CAM5 ~~MIROC4h~~ simulate the smallest dust emission area, which are 2-3% of the global  
490 surface area, while CanESM2 simulates the largest dust emission area (18% of the global  
491 surface area; Figure 4-6 and Table 3). The maximum normalized dust emission flux is  
492 also the largest at ~~3635~~ ~~2682~~ and ~~2682~~ ~~3635~~ in MIROC4h ~~CESM1-CAM5~~ and CESM1-  
493 CAM5 ~~MIROC4h~~, respectively, indicating the “hot spots” with extremely high dust  
494 emission flux in the two models. The maximum normalized dust emission flux is  
495 generally between 100 and 300 in other CMIP5 models and is approximately 200 in  
496 MERRA-2 reanalysis.

497 The smallest dust emission area in CESM1-CAM5 is mainly because the model  
498 adopts a geomorphic source erodibility with ~~a-its~~ threshold value of 0.1 for the dust  
499 emission occurrences (Zender et al., 2003; Wu et al., 2016). Small dust emission area in  
500 MIROC4h may be ~~mainly~~ ~~partly~~ due to the weaker surface winds in MIROC4h compared

设置了格式: 字体: 加粗

带格式的: 列表段落, 缩进: 左侧: 0 厘米, 首行缩进:  
0 字符, 多级符号 + 级别: 3 + 编号样式: 1, 2, 3,  
... + 起始编号: 1 + 对齐方式: 左侧 + 对齐位置: 1.5  
厘米 + 缩进位置: 2.5 厘米

501 to other three MIROC family models (MIROC5, MIROC-ESM, MIROC-ESM-CHEM)  
502 (Figure 5e-5f). In the dust source regions (normalized dust emission flux >0.01), the  
503 annual mean surface wind speeds are 3.7, 4.4, 4.1, and 4.1 m s<sup>-1</sup>, respectively in  
504 MIROC4h, MIROC5, MIROC-ESM and MIROC-ESM-CHEM. MIROC4h differs much  
505 from other three MIROC models in both dynamic core and physical parameterizations  
506 (Watanabe et al., 2010, 2011; Sakamoto et al., 2011), which can explain the weakest  
507 surface winds in MIROC4h, higher horizontal resolution of the model (0.56°) than other  
508 models (1°-3°) including MIROC5 (Table 1). The higher model resolution may change  
509 the patterns of wind speeds and precipitation as well as the occurrence frequency of  
510 strong winds and heavy precipitation and thus affect the dust emission regions. In North  
511 Hemisphere, MIROC4h adopts a larger leaf area index than MIROC5, which can also  
512 lead to the smaller dust emission area in MIROC4h (Figure 5a-5b). The largest dust  
513 emission area in CanESM2 may be due to its prescribed land cover map, and/or adoption  
514 of gustiness adjustment for wind friction velocity (von Salzen et al., 2013). MERRA-2  
515 gives a value of 7.4% for the dust emission area, which is in the median of all the CMIP5  
516 model results. Note GFDL-CM3 and CSIRO-Mk3-6.0, which adopt the same dust  
517 emission scheme and source erodibility (Section 2), show similar dust emission regions.

518 As normalized dust emission flux is comparable among the CMIP5 models, a global  
519 map of multi-model mean and standard deviation of normalized dust emission flux are  
520 thus constructed and shown in Figure 57. The multi-model mean represents the general  
521 consensus among the CMIP5 models while the standard deviation indicates the  
522 variability among models. The relative standard deviation is calculated by the ratio of  
523 standard deviation to the mean, which is shown to illustrate the uncertainty among the

设置了格式: 上标

设置了格式: 非突出显示

524 models. Mean normalized dust emission flux is large ( $>10$ ) in the desert regions in North  
525 Africa, Middle East, Central Asia, South Asia, East Asia, and Australia (Figure 5a7a). It  
526 ranges from 1-10 in the desert adjacent regions and in small regions of South America,  
527 North America, and South Africa (Figure 5a7a). The patterns of standard deviation of  
528 multi-model results are generally similar to those of mean normalized dust emission flux  
529 (Figure 5b7b). However, the relative standard deviation is quite different from the mean  
530 normalized dust emission flux, and its pattern is nearly opposite (Figure 5c7c). The  
531 relative standard deviation is mostly below 1 in the aforementioned desert regions with  
532 larger mean normalized dust emission ( $>10$ ) and increases to 1-4 in other regions with  
533 relative smaller dust emission, indicating the large uncertainty of estimated dust emission  
534 flux in the CMIP5 models.

535       Difference of dust emission uncertainty in different regions can be explained by two  
536 reasons. First, in the deserts, soil is extremely dry (below the criteria for dust emission)  
537 and surface is covered with little vegetation. In these regions, the models agree with each  
538 other more easily in simulating the occurrence of dust emission. In the regions adjacent to  
539 the deserts or with localized sandy lands, where soil is wetter and there is more  
540 vegetation cover at the surface, the models differ significantly in the parameterizations of  
541 dust emission, treatment of land cover, and simulated meteorology, and thus climate  
542 models differ in their estimation of dust emission more strongly. Second, there are a  
543 larger variety of complexities in the CMIP5 models compared to the models participating  
544 in the AeroCom intercomparison (Section 2). Some models use the dynamic vegetation  
545 for dust emission (e.g., HadGEM2-CC/ES, MIROC-ESM, MIROC-ESM-CHEM), and  
546 deviate largely from other models over the regions with sparse vegetation cover such as

547 Australia. This further increases the differences in dust emission among the CMIP5  
548 models.

549

### 550 **4.3 Dust deposition flux**

551 Dust deposition is a vital process in the dust cycle which removes dust particles  
552 from the atmosphere and provides nutrients to the terrestrial and marine ecosystems.

553 Figure 86 shows the comparison of dust deposition flux at 84 selected stations between  
554 the models and observations. Only seven CMIP5 models provide total dust deposition  
555 flux (sum of dry and wet deposition), which are used here. The global dust emission in  
556 these seven models ranges from 1600 to 3500 Tg yr<sup>-1</sup>, which is at the medium level of all  
557 the CMIP5 models. Observed annual mean dust deposition flux ranges from 10<sup>-4</sup> to 10<sup>3</sup> g  
558 m<sup>-2</sup> yr<sup>-1</sup>, indicating large spatial variabilities of dust deposition. In general, six of seven  
559 CMIP5 models (excluding ACCESS1-0) reproduces the observed dust deposition flux  
560 within a factor of 10 in most regions except over the Southern Ocean, Antarctica, and  
561 Pacific. Over the Southern Ocean and in the Antarctica, all the models except CESM1-  
562 CAM5 overestimate the dust deposition flux by more than a factor of 10 at two stations.  
563 Over the Pacific Ocean, all the models except CanESM2 underestimate the dust  
564 deposition flux by more than 10 times at several stations. In addition to the  
565 overestimation over the Southern Ocean and Antarctica and the underestimation over the  
566 Pacific Ocean, ACCESS1-0 mostly underestimate the dust deposition flux in other  
567 regions with underestimation by more than a factor of 10 at several stations. Overall  
568 ACCESS1-0 underestimates the dust deposition flux by approximately a factor of 2 on  
569 average.



570 Similar to most of the CMIP5 models, MERRA-2 reproduces the observed dust  
571 deposition flux within a factor of 10 at most stations except over the Southern Ocean and  
572 Antarctica. Over the Southern Ocean and Antarctica, MERRA-2 tends to overestimate  
573 the dust deposition flux by more than a factor of 10 at most stations. Compared to the  
574 CMIP5 models, larger dust deposition over the Southern Ocean and Antarctica in  
575 MERRA-2 may be related to the adoption of both meteorology and aerosol assimilation  
576 in MERRA-2, which affects the dust transport and deposition. As mentioned in Section 2,  
577 only AOD is taken into account in the aerosol assimilation for MERRA-2. Therefore the  
578 large discrepancy of dust deposition at several stations in MERRA-2 may result from the  
579 unrealistic representation of dust vertical profiles, size distribution, and deposition  
580 process. Overall, the correlation coefficients between CMIP5 models and observations  
581 (after taking the logarithms of both them;  $R_{\log}$ ) range from 0.90 to 0.92 and are slightly  
582 higher than that of MERRA-2 (0.87). The model biases may result from inaccurate  
583 representation of underlying model processes such as dust emission, transport, and  
584 deposition. The biases may also be partly explained by the consistency between the  
585 observations and simulations, especially for those observation which were made at a  
586 relatively short-term period (one to several years), as mentioned in Section 3.1.

587 ~~Dust deposition includes two mechanisms: dry and wet deposition. Figure 7 shows~~  
588 ~~the comparison of fraction of wet deposition in total deposition from models and~~  
589 ~~observations at 10 stations. These stations are located downwind of dust sources and can~~  
590 ~~be classified into two groups. One group are Bermuda (station #1) over the western~~  
591 ~~Atlantic Ocean, Amsterdam Island (station #2) over the southern Indian Ocean, Cape~~  
592 ~~Ferrat (station #3) in southern Europe, and New Zealand (station #6). For this group of~~

593 stations, fractions of wet deposition range from 17% to 70%. At these stations, all the  
594 models simulate the fractions of wet deposition exceeding 75% and significantly  
595 overestimate the fractions of wet deposition. MERRA-2 estimates smaller fractions of  
596 wet deposition compared to the CMIP5 models but still significantly overestimates  
597 fractions of wet deposition at these stations.

598 The other group includes Enewetak Atoll (station #4), Samoa (station #5) and  
599 Fanning (station #8) over the tropical Pacific Ocean, Midway (station #7) over the  
600 subtropical Pacific Ocean, Greenland (station #9) and Coastal Antarctica (station #10) in  
601 the high latitudes. These stations are thousands of kilometers away from sources. At these  
602 stations, observed fractions of wet deposition range from 65% to 90%, indicating the  
603 dominance of wet deposition. Most of CMIP5 models except CanESM2 simulate the  
604 fractions of wet deposition within 20% of observations. CanESM2 also simulates the  
605 fraction of wet deposition comparable to observations except at Coastal Antarctica where  
606 CanESM2 underestimates the fraction of wet deposition by up to 35%. MERRA-2  
607 captures well the fraction of wet deposition over the tropical and subtropical Pacific  
608 Ocean but significantly underestimate it by 40-45% in the high latitudes. The large  
609 underestimation by CanESM2 and MERRA-2 may be related to the meteorology such as  
610 precipitation and turbulent flux, or the parameterizations of dust deposition in the models,  
611 which deserves future investigations.

612 Dust cycle can deliver nutrients from continents to oceans. Table 5 summarizes the  
613 dust deposition and fraction of wet deposition onto the global surface, continents and  
614 oceans, respectively in seven CMIP5 models and MERRA-2 reanalysis. Total deposition  
615 in continents ranges from 1331 to 2850 Tg yr<sup>-1</sup> in seven CMIP5 models and accounts for

616 77-91 % of global total deposition. Total deposition in all the oceans ranges from 197 to  
617 686 Tg yr<sup>-1</sup> and accounts for 9-23 % of global total deposition, indicating a considerable  
618 uncertainty in dust deposition, which should be taken into account in modeling the  
619 marine biogeochemistry with ESMs. It is interesting to mention that if ACCESS1-0 with  
620 largest dust particle size range (0.06-63 μm in diameter) and largest fraction (91%) for  
621 continental deposition is excluded, other six models simulate quite similar fraction of  
622 continental deposition (78-83%). MERRA-2 estimates 71% (29%) of dust deposited in  
623 continents (oceans), and this estimation is smaller (larger) than all seven CMIP5 models,  
624 indicating MERRA-2 transport dust more efficiently to oceans. This is consistent with the  
625 comparison of dust deposition flux shown in Figure 86 and may be related to the  
626 assimilation of both meteorology and aerosols in MERRA-2. The fractions of wet  
627 deposition (with respect to total deposition) in seven CMIP5 models are 8-33% and 49-71%  
628 over continents and oceans, respectively. MERRA-2 estimates the fraction of wet  
629 deposition (with respect to total deposition) 26% and 69% over the continents and oceans,  
630 respectively, which lie within the range of CMIP5 models.

631

#### 632 4.4 Surface dDust concentration

633 Dust concentration is an important variable for its cycle. Figure 98 shows the  
634 comparison of surface dust concentrations between models and observations at 22  
635 selected stations. These stations are located in the downwind regions of dust sources, and  
636 annual mean dust concentrations at these stations range from 10<sup>-1</sup> to 10<sup>2</sup> μg m<sup>-3</sup>. In  
637 general, the models reproduce observed surface dust concentrations within a factor of 10,  
638 with the exceptions of HadGEM2-CC/ES and MIROC4h. Although HadGEM2-CC/ES

639 simulate well observed surface dust concentrations at the stations over the Atlantic Ocean  
640 (stations #1-4) and slightly underestimate the observations in East Asia (stations #7-8),  
641 the two models significantly overestimate surface dust concentrations at most of other  
642 stations especially at the station located in Australia and downwind regions (stations  
643 #15-21). This is consistent with their much higher dust emission in Australia compared to  
644 other models (Table 3; Section 4.2). This is also consistent with the overestimation of  
645 dust optical depth in Australia by HadGEM2-CC/ES compared to satellite observations  
646 (Pu and Ginoux, 2018). In contrast, MIROC4h largely underestimates surface dust  
647 concentrations by 1-2 orders of magnitude at most stations. Although compared to  
648 MIROC5, MIROC4h only simulates approximately 4 times lower global dust emission,  
649 MIROC4h tends to concentrate all the dust emissions over smaller regions of global  
650 surface (2.9% compared to 6.1%). Therefore, dust is less widely distributed in the  
651 atmosphere and a smaller fraction of dust is transported to the downwind regions in  
652 MIROC4h, as indicated by its almost 8 times smaller dust burden and only half the dust  
653 lifetime compared to MIROC5. This difference can explain lower surface dust  
654 concentrations in MIROC4h. Another reason may lie in the vertical diffusion of dust,  
655 which also determines the distance of its horizontal transport.

656 Although the CMIP5 models (excluding HadGEM2-CC/ES ~~MIROC4h~~ and  
657 ~~MIROC4h-HadGEM2-CC/ES~~) can roughly reproduce the observed magnitudes of  
658 surface dust concentrations at most stations, considerable discrepancy between models  
659 and observations can be found at certain regions. Most models except CanESM2  
660 significantly underestimate dust concentrations at stations in Antarctica (stations #21 and  
661 #22), with the largest underestimation by more than 2 orders of magnitude in MIROC-

662 ESM/MIROC-ESM-CHEM which also simulates much lower dust emissions in Australia,  
663 South Africa, and southeastern South America (Figure 3; Section 4.2). Eight models  
664 (ACCESS1-0, ~~CESM-CAM5, CSIRO-Mk3-6-0~~, GFDL-CM3, GISS-E2-H/R, MRI-  
665 CGCM3, MRI-ESM1, ~~CESM-CAM5, CSIRO-Mk3-6-0~~) largely underestimate dust  
666 concentrations by 1-2 orders of magnitude at station #6 in South Africa. Three MIROC  
667 family models (MOROC5, MOROC-ESM, MIROC-ESM-CHEM) underestimate dust  
668 concentrations by 1-2 orders of magnitude at several stations in the downwind regions of  
669 Australia (stations #14, 15, and 17). Other noticeable discrepancies include  
670 underestimations in East Asia by ACCESS1-0/MIROC5, underestimations over the  
671 Tropical Pacific Ocean by CESM-CAM5/GISS-H2-H/GISS-E2-R, and overestimations  
672 in Australia by CanESM2.

673 Overall the correlation coefficients and mean biases between CMIP5 models and  
674 observations (after taking the logarithms of both of them;  $R_{\log}$  and  $MB_{\log}$ ) ranges from  
675 0.55 to 0.88 and from -5.59 to 1.52 for all CMIP5 models, respectively. All the  
676 correlation coefficients are statistically significant at the 0.005 level. If HadGEM2-  
677 CC/ES and MIORC4h are excluded for the calculation,  $R_{\log}$  and  $MB_{\log}$  range from 0.60 to  
678 0.88 and from -1.61 to 1.04, respectively. As a  $MB_{\log}$  of -0.7 (0.7) corresponds to a  
679 general underestimation (overestimation) by a factor of 2, six models (~~CESM1-CAM5,~~  
680 ~~GISS-E2-H/R,~~ MIROC5, MIROC-ESM, MIROC-ESM-CHEM, ~~CESM1-CAM5, GISS-~~  
681 ~~E2-H/R~~) underestimate surface dust concentrations by more than a factor of 2 on average,  
682 while CanESM2 overestimates surface dust concentrations by the similar magnitude.

683 Compared to observations, MERRA-2 simulates well the dust concentrations at all  
684 stations except station #6 in South Africa. This improvement by MERRA-2 compared to

685 the CMIP5 models may be due to the inclusion of both meteorology and aerosol  
686 assimilation in MERRA-2. The correlation coefficients ( $R_{\log}$ ) between MERRA-2 and  
687 observations is 0.91, which is larger than all the CMIP5 models, and mean bias ( $MB_{\log}$ ) is  
688 close to zero (0.01).

689

## 690 **5. Discussion and Conclusions**

691 In this study we examine the present-day global dust cycle simulated by the 15  
692 climate models participating in the CMIP5 project. The simulations are also compared  
693 with a dataset MERRA-2 and observations of dust deposition and concentration. The  
694 results show that the global dust emission in these models ~~ranges-differs much:~~ from ~~735~~  
695 2218 to 8186 Tg yr<sup>-1</sup> (size range of 0.06-63 μm in diameter), from 735 to 3598 Tg yr<sup>-1</sup>  
696 (size range of 0.06-20 μm in diameter), and from 1677 to 3698 Tg yr<sup>-1</sup> (size <16 μm in  
697 diameter)and the global dust burden ranges from 2.5 to 41.9 Tg. The differences are  
698 larger than those from models participating in the AeroCom project (Huneeus et al.,  
699 2011), which is a result of enhanced model complexities in modeling both climate and  
700 dust emission in the CMIP5 modelsglobal dust emission ranges by a factor of 4-5 for dust  
701 particles in the same size range.

702 The simulated dust emission regions also differ greatly accounting for a global  
703 surface area of 2.9%-18%. The models agree most with each other in reproducing the  
704 “dust belt” that extends from North Africa, Middle East, Central Asia, South Asia, to East  
705 Asia, but there are large uncertainties in the extent of this “dust belt” and other source  
706 regions including Australia, North America, South America, and South Africa.  
707 Particularly, some models simulate little dust emissions (<0.1% of global dust emission)

708 in Australia and North America, while some other models simulate larger dust emissions  
709 there which account for 10-30% and 3-4% of global dust emission in Australia and North  
710 America, respectively. It is also revealed that the increasing complexity of ESMs  
711 (HadGEM2-CC/ES, MIROC-ESM, and MIROC-ESM-CHEM) by coupling dust  
712 emission with dynamic vegetation can amplify the uncertainty associated with dust  
713 emissions.

714 Removal of dust particles in the CMIP5 models is mainly through dry deposition,  
715 and wet deposition only accounts for 12-39% of total deposition. The associated dust life  
716 time is about 1.3-4.4 days. A clear linear relationship between dust burden, dust lifetime,  
717 and fraction of wet deposition to total deposition is present in the CMIP5 models,  
718 suggesting a general consistency among these models. The models also estimate that 77-  
719 91% of emitted dust are deposited back to continents and 9-23% of them are deposited to  
720 the oceans. The fraction of wet deposition is smaller in most CMIP5 models and dust  
721 lifetime is shorter compared to MERRA-2 reanalysis, indicating a shorter distance for  
722 dust transport from its sources in most CMIP5 models. Compared to the observations, the  
723 CMIP5 models (except MIRCO4h) reproduce dust deposition flux and surface dust  
724 concentration by a factor of 10 at most stations. Larger discrepancies are found in the  
725 remote regions such as Antarctica and Tropical Pacific Ocean. In Australia and  
726 downwind regions, four MIROC family models (MIROC4h, MIROC5, MIROC-ESM,  
727 MIROC-ESM-CHEM) which simulate little dust emission in Australia largely  
728 underestimate the dust concentrations at stations in the remote regions. Contrarily  
729 HadGEM2-CC/ES overestimate dust concentrations. MIROC4h shows the largest  
730 discrepancy by underestimating the surface dust concentrations by more than a factor of

731 100 in Australia and downwind regions. Overall, although MIROC4h simulates 4-5 times  
732 lower global dust emission than other three MIROC family models, MIROC4h simulates  
733 on average more than 50 times smaller surface dust concentrations at 22 stations. This  
734 can be ascribed to the fact that most dust emissions in MIROC4h are concentrated over  
735 the desert centers, which limits the long-range transport of dust particles to the remote  
736 regions.

737 These results show large uncertainties of global dust cycle in ESMs. In fact, these  
738 models are fully-coupled atmosphere-land-ocean models and some of them also include  
739 the dynamic vegetation. As a result, in several key regions such as Australia and North  
740 America, uncertainties are larger compared to those in previous models participating in  
741 the AeroCom intercomparison project where sea surface temperature is prescribed, and  
742 more strictly, in some models, meteorological fields are prescribed from reanalysis  
743 (Huneeus et al., 2011). Larger uncertainties in the CMIP5 models with dynamic  
744 vegetation is expected, as a prognostic vegetation would depart from the observed or  
745 constructed vegetation and may also lead to a large bias in soil moisture, which may thus  
746 lead to an additional bias in dust emissions in these models. Uncertainties of dust  
747 simulations also vary with regions, and a smaller uncertainty is found in the deserts over  
748 the “dust belt” in the North Hemisphere, but a larger uncertainty exists in other regions  
749 including Australia and North America. The large uncertainties of global dust cycle in the  
750 CMIP5 models would cast a doubt on the reliability of dust radiative forcing estimated in  
751 these models. Future work is therefore needed to identify the sources of these  
752 uncertainties and improve global dust cycle in climate models.

753



754 **6. Future work**

755 Because the dust lifecycle involves various processes with the scales from  
756 micrometers to tens of thousands of kilometers and consists of lots of parameters, the  
757 representation of dust cycle in climate models is a big challenge for the model  
758 community. Dust emission is the first and foremost process for model improvements of  
759 dust cycle (Shao, 2008; Shao et al., 2011). Improving dust emission not only lies in the  
760 development of dust emission scheme but also in its implementation into climate models  
761 (e.g., Shao, 2008; Wu et al., 2016; Wu et al., 2019). For example, different dust emission  
762 schemes with specific land cover datasets and criteria for the occurrence of dust emission  
763 are adopted in the models (Table 1 and references therein). Therefore, different results of  
764 dust emission among the CMIP5 models reflect the uncertainty in many aspects of the  
765 model, including the differences in meteorology, soil moisture, land cover data, and dust  
766 emission parameterizations, as in many previous intercomparison studies (e.g., Uno et al.,  
767 2006; Textor et al., 2006; Todd et al., 2008; Huneeus et al., 2011). A close look at these  
768 factors in each model will help to unravel reasons behind the biases in these models. In  
769 addition, it is also helpful to setup more constrained experiments to separate the  
770 sensitivity of model estimates to individual factors, by varying one single factor such as  
771 dust emission scheme (e.g., Wu and Lin, 2013) and land surface scheme (e.g., Lin et al.,  
772 2012), or using identical emissions (e.g., Textor et al., 2007).

773 In this study, in addition, the models are only evaluated with observed dust deposition  
774 and surface concentrations. Some of these observations, however, were made at a  
775 relatively short period with one to several years and insufficient to represent current  
776 climatology, which may partly contribute to model discrepancies (Section 4). It is

设置了格式: 字体: 加粗

带格式的: 列表段落, 首行缩进: 0 字符, 多级符号 + 级别: 1 + 编号样式: 1, 2, 3, ... + 起始编号: 1 + 对齐方式: 左侧 + 对齐位置: 0 厘米 + 缩进位置: 0.63 厘米

设置了格式: 字体: 加粗

777 desirable to collect a long-term dataset. Although it is roughly acceptableMoreover, it is  
778 also desirable to collect the observations of dust emission flux and use them for model  
779 evaluation. Particularly, for dust deposition and dust concentration, some biases come  
780 from dust emission and others from circulation and deposition parameterizations. It is  
781 only possible to separate the contributions of different processes to the biases in dust  
782 deposition and concentration, if observations of dust emission are also included in model  
783 comparison. In addition, a dust aerosol reanalysis could serve a benchmark data to  
784 evaluate model performance. However, the current aerosol reanalysis is still not sufficient  
785 for a comprehensive evaluation of dust cycle (Section 3.2). In particular, because of the  
786 limitation in dust emission, we are unable to analyze the contribution of different factors  
787 such as meteorological fields and land surface states to biases in dust emission. It is  
788 desirable that future aerosol reanalysis also includes adjoint inversion of dust emissions  
789 using more specific observations such as lidar observations as done in Yumimoto et al.  
790 (2007).

791 We have compared the global dust emission and burden among the models with the  
792 same dust size range considered. It should be mentioned that dust size distribution is an  
793 important parameter for dust cycle (e.g., Shao, 2008; Mahowald et al., 2014), and it is not  
794 included in this study as the model data are not available. Evolution of dust size  
795 distribution during dust transport and deposition is critical to our understanding of the  
796 model bias in dust cycle. We suggest that the size-resolved dust emission, concentration,  
797 and deposition should be outputted and provided in the latest CMIP6 project (Eyring et  
798 al., 2016). Moreover, observations of size-resolved dust concentration and deposition is

设置了格式: 字体: (中文) MyriadPro

799 urgently needed. A compile of available observations of dust size distribution (e.g.,  
800 Mahowald et al., 2014; Ryder et al., 2018) are also required for model evaluation.

801

#### 802 **Data availability**

803 CMIP5 results are available in <https://esgf-node.llnl.gov/search/cmip5/>. MERRA-2  
804 is available in <https://disc.gsfc.nasa.gov/datasets?project=MERRA-2>. Observations of  
805 dust deposition and fraction of wet deposition is provided in the literature led by N.  
806 Huneus (<https://www.atmos-chem-phys.net/11/7781/2011/>). Observations of surface  
807 dust concentrations are provided by Joseph M. Prospero from the Rosenstiel School of  
808 Marine and Atmospheric Science at the University of Miami.

809

#### 810 **Author contributions**

811 CW and ZL designed the study. CW did the data analyses with advices from ZL and  
812 XL. CW wrote the manuscript with contributions from ZL and XL.

813

#### 814 **Competing interests**

815 The authors declare that they have no conflict of interest.

816

#### 817 **Acknowledgement**

818 This research is jointly supported by the National Natural Science Foundation of  
819 China (grant 41975119 and 41830966), Chinese Academy of Sciences (CAS) Strategic  
820 Priority Research Program (grant XDA19030403), and CAS The Belt and Road  
821 Initiatives Program on International Cooperation (grant 134111KYSB20060010). C. Wu

822 is supported by the CAS Pioneer Hundred Talents Program for Promising Youth (Class  
823 C). We acknowledge the WCRP's Working Group on Coupled Modelling, which is  
824 responsible for CMIP, and the various climate modeling groups for producing and  
825 making available their model output. We also thank the team for generating MERRA-2  
826 data and make them available. We also thank Prof. Joseph M. Prospero for providing the  
827 observations of surface dust concentrations and helpful discussions.

828

## 829 **References**

- 830 Adachi, Y., Yukimoto, S., Deushi, M., Obata, A., Nakano, H., Tanaka, T. Y., et al.: Basic  
831 performance of a new earth system model of the Meteorological Research Institute  
832 (MRI-ESM 1). *Papers in Meteorology and Geophysics*, 64, 1-19,  
833 <https://doi.org/10.2467/mripapers>, 2013.
- 834 Arora, V. K., Scinocca, J. F., Boer, G. J., Christian, J. R., Denman, K. L., Flato, G. M.,  
835 Kharin, V. V., Lee, W. G., and Merryfield, W. J.: Carbon emission limits required to  
836 satisfy future representative concentration pathways of greenhouse gases, *Geophys*  
837 *Res Lett*, 38, <https://doi.org/10.1029/2010GL046270>, 2011.
- 838 Bell, M. L., Levy, J. K., and Lin, Z.: The effect of sandstorms and air pollution on cause-  
839 specific hospital admissions in Taipei, Taiwan, *Occup Environ Med*, 65, 104-111,  
840 <https://doi.org/10.1136/oem.2006.031500>, 2008.
- 841 Bellouin, N., Rae, J., Jones, A., Johnson, C., Haywood, J., and Boucher, O.: Aerosol  
842 forcing in the Climate Model Intercomparison Project (CMIP5) simulations by  
843 HadGEM2-ES and the role of ammonium nitrate, 116,  
844 <https://doi.org/10.1029/2011jd016074>, 2011.
- 845 Bi, D., Dix, M., Marsland, S., O' Farrell, S., Rashid, H., Uotila, P., et al.: The ACCESS  
846 Coupled Model: Description, control climate and evaluation. *Australian*  
847 *Meteorological and Oceanographic Journal*, 63(1), 41-64, 10.22499/2.6301.004,  
848 2013.
- 849 Boucher, O., Randall, D., Artaxo, P., Bretherton, C., Feingold, G., Forster, P., Kerminen,  
850 V.-M., Kondo, Y., Liao, H., and Lohmann, U.: Clouds and aerosols, in: *Climate*  
851 *change 2013: the physical science basis. Contribution of Working Group I to the*  
852 *Fifth Assessment Report of the Intergovernmental Panel on Climate Change*,  
853 Cambridge University Press, 571-657, 2013.

854 Buchard, V., Randles, C. A., Silva, A. M. d., Darmenov, A., Colarco, P. R., Govindaraju,  
855 R., Ferrare, R., Hair, J., Beyersdorf, A. J., Ziemba, L. D., and Yu, H.: The MERRA-2  
856 Aerosol Reanalysis, 1980 Onward. Part II: Evaluation and Case Studies, 30, 6851-  
857 6872, <https://doi.org/10.1175/jcli-d-16-0613.1>, 2017.

858 Bullard, J. E., Baddock, M., Bradwell, T., Crusius, J., Darlington, E., Gaiero, D., Gassó,  
859 S., Gisladdottir, G., Hodgkins, R., McCulloch, R., McKenna-Neuman, C., Mockford,  
860 T., Stewart, H., and Thorsteinsson, T.: High-latitude dust in the Earth system, 54,  
861 447-485, <https://doi.org/10.1002/2016rg000518>, 2016.

862 Cakmur, R. V., Miller, R. L., Perlwitz, J., Geogdzhayev, I. V., Ginoux, P., Koch, D.,  
863 Kohfeld, K. E., Tegen, I., and Zender, C. S.: Constraining the magnitude of the  
864 global dust cycle by minimizing the difference between a model and observations,  
865 *Journal of Geophysical Research: Atmospheres*, 111,  
866 <https://doi.org/doi:10.1029/2005JD005791>, 2006.

867 Collins, W. J., Bellouin, N., Doutriaux-Boucher, M., Gedney, N., Halloran, P., Hinton, T.,  
868 Hughes, J., Jones, C. D., Joshi, M., Liddicoat, S., Martin, G., O'Connor, F., Rae, J.,  
869 Senior, C., Sitch, S., Totterdell, I., Wiltshire, A., and Woodward, S.: Development  
870 and evaluation of an Earth-System model – HadGEM2, *Geosci. Model Dev.*, 4,  
871 1051-1075, <https://doi.org/10.5194/gmd-4-1051-2011>, 2011.

872 Delworth, T. L., Broccoli, A. J., Rosati, A., Stouffer, R. J., Balaji, V., Beesley, J. A.,  
873 Cooke, W. F., Dixon, K. W., Dunne, J., Dunne, K. A., Durachta, J. W., Findell, K. L.,  
874 Ginoux, P., Gnanadesikan, A., Gordon, C. T., Griffies, S. M., Gudgel, R., Harrison,  
875 M. J., Held, I. M., Hemler, R. S., Horowitz, L. W., Klein, S. A., Knutson, T. R.,  
876 Kushner, P. J., Langenhorst, A. R., Lee, H.-C., Lin, S.-J., Lu, J., Malyshev, S. L.,  
877 Milly, P. C. D., Ramaswamy, V., Russell, J., Schwarzkopf, M. D., Shevliakova, E.,  
878 Sirutis, J. J., Spelman, M. J., Stern, W. F., Winton, M., Wittenberg, A. T., Wyman, B.,  
879 Zeng, F., and Zhang, R.: GFDL's CM2 Global Coupled Climate Models. Part I:  
880 Formulation and Simulation Characteristics, *J Climate*, 19, 643-674,  
881 <https://doi.org/10.1175/jcli3629.1>, 2006.

882 Dix, M., Vohralik, P., Bi, D., Rashid, H., Marsland, S., O'Farrell, S., et al.: The ACCESS  
883 Coupled Model: Documentation of core CMIP5 simulations and initial results.  
884 *Australian Meteorological and Oceanographic Journal*, 63(1), 83-99,  
885 10.22499/2.6301.005, 2013.

886 Donner, L. J., Wyman, B. L., Hemler, R. S., Horowitz, L. W., Ming, Y., Zhao, M., Golaz,  
887 J.-C., Ginoux, P., Lin, S.-J., Schwarzkopf, M. D., Austin, J., Alaka, G., Cooke, W. F.,  
888 Delworth, T. L., Freidenreich, S. M., Gordon, C. T., Griffies, S. M., Held, I. M.,  
889 Hurlin, W. J., Klein, S. A., Knutson, T. R., Langenhorst, A. R., Lee, H.-C., Lin, Y.,  
890 Magi, B. I., Malyshev, S. L., Milly, P. C. D., Naik, V., Nath, M. J., Pincus, R.,

891 Ploshay, J. J., Ramaswamy, V., Seman, C. J., Shevliakova, E., Sirutis, J. J., Stern, W.  
892 F., Stouffer, R. J., Wilson, R. J., Winton, M., Wittenberg, A. T., and Zeng, F.: The  
893 Dynamical Core, Physical Parameterizations, and Basic Simulation Characteristics  
894 of the Atmospheric Component AM3 of the GFDL Global Coupled Model CM3, *J*  
895 *Climate*, 24, 3484-3519, <https://doi.org/10.1175/2011jcli3955.1>, 2011.

896 Evan, A. T., Flamant, C., Fiedler, S., and Doherty, O.: An analysis of aeolian dust in  
897 climate models, *Geophys Res Lett*, 41, 5996-6001, 10.1002/2014GL060545, 2014.

898 Eyring, V., Bony, S., Meehl, G. A., Senior, C. A., Stevens, B., Stouffer, R. J., and Taylor,  
899 K. E.: Overview of the Coupled Model Intercomparison Project Phase 6 (CMIP6)  
900 experimental design and organization, *Geosci. Model Dev.*, 9, 1937-1958,  
901 <https://doi.org/10.5194/gmd-9-1937-2016>, 2016.

902 Flato, G., Marotzke, J., Abiodun, B., Braconnot, P., Chou, S.C., Collins, W., Cox, P.,  
903 Driouech, F., Emori, S., Eyring, V., Forest, C., Gleckler, P., Guilyardi, E., Jakob, C.,  
904 Kattsov, V., Reason, C. and Rummukainen, M.: Evaluation of Climate Models. In:  
905 *Climate Change 2013: The Physical Science Basis. Contribution of Working Group I*  
906 *to the Fifth Assessment Report of the Intergovernmental Panel on Climate Change*,  
907 Cambridge University Press, Cambridge, United Kingdom, 741-866, 2013.

908 Formenti, P., Schutz, L., Balkanski, Y., Desboeufs, K., Ebert, M., Kandler, K., Petzold, A.,  
909 Scheuven, D., Weinbruch, S., and Zhang, D.: Recent progress in understanding  
910 physical and chemical properties of African and Asian mineral dust, *Atmos Chem*  
911 *Phys*, 11, 8231-8256, <https://doi.org/10.5194/acp-11-8231-2011>, 2011.

912 Forster, P., et al., Changes in atmospheric constituents and in radiative forcing, in *Climate*  
913 *Change 2007: The Physical Science Basis. Contribution of Working Group I to the*  
914 *Fourth Assessment Report of the Intergovernmental Panel on Climate Change*,  
915 edited by S. Solomon et al., Cambridge Univ. Press, Cambridge, U. K, 129-234,  
916 2007.

917 Gelaro, R., McCarty, W., Suárez, M. J., Todling, R., Molod, A., Takacs, L., Randles, C. A.,  
918 Darmenov, A., Bosilovich, M. G., Reichle, R., Wargan, K., Coy, L., Cullather, R.,  
919 Draper, C., Akella, S., Buchard, V., Conaty, A., Silva, A. M. d., Gu, W., Kim, G.-K.,  
920 Koster, R., Lucchesi, R., Merkova, D., Nielsen, J. E., Partyka, G., Pawson, S.,  
921 Putman, W., Rienecker, M., Schubert, S. D., Sienkiewicz, M., and Zhao, B.: The  
922 Modern-Era Retrospective Analysis for Research and Applications, Version 2  
923 (MERRA-2), 30, 5419-5454, <https://doi.org/10.1175/jcli-d-16-0758.1>, 2017.

924 Ginoux, P., Chin, M., Tegen, I., Prospero, J. M., Holben, B., Dubovik, O., and Lin, S. J.:  
925 Sources and distributions of dust aerosols simulated with the GOCART model, *J*  
926 *Geophys Res-Atmos*, 106, <https://doi.org/20255-20273>, 2001.

927 Ginoux, P., Prospero, J. M., Torres, O., and Chin, M.: Long-term simulation of global

928 dust distribution with the GOCART model: correlation with North Atlantic  
929 Oscillation, *Environ Modell Softw*, 19, 113-128, [https://doi.org/10.1016/S1364-](https://doi.org/10.1016/S1364-8152(03)00114-2)  
930 [8152\(03\)00114-2](https://doi.org/10.1016/S1364-8152(03)00114-2), 2004.

931 Ginoux, P., Prospero, J. M., Gill, T. E., Hsu, N. C., and Zhao, M.: Global-Scale  
932 Attribution of Anthropogenic and Natural Dust Sources and Their Emission Rates  
933 Based on Modis Deep Blue Aerosol Products, *Rev Geophys*, 50, Artn Rg3005,  
934 <https://doi.org/10.1029/2012rg000388>, 2012.

935 Huneus, N., Schulz, M., Balkanski, Y., Griesfeller, J., Prospero, J., Kinne, S., Bauer, S.,  
936 Boucher, O., Chin, M., Dentener, F., Diehl, T., Easter, R., Fillmore, D., Ghan, S.,  
937 Ginoux, P., Grini, A., Horowitz, L., Koch, D., Krol, M. C., Landing, W., Liu, X.,  
938 Mahowald, N., Miller, R., Morcrette, J. J., Myhre, G., Penner, J., Perlwitz, J., Stier,  
939 P., Takemura, T., and Zender, C. S.: Global dust model intercomparison in AeroCom  
940 phase I, *Atmos Chem Phys*, 11, 7781-7816, [https://doi.org/10.5194/acp-11-7781-](https://doi.org/10.5194/acp-11-7781-2011)  
941 [2011](https://doi.org/10.5194/acp-11-7781-2011), 2011.

942 Hurrell, J. W., Holland, M. M., Gent, P. R., Ghan, S., Kay, J. E., Kushner, P. J., Lamarque,  
943 J. F., Large, W. G., Lawrence, D., Lindsay, K., Lipscomb, W. H., Long, M. C.,  
944 Mahowald, N., Marsh, D. R., Neale, R. B., Rasch, P., Vavrus, S., Vertenstein, M.,  
945 Bader, D., Collins, W. D., Hack, J. J., Kiehl, J., and Marshall, S.: The Community  
946 Earth System Model: A Framework for Collaborative Research, *Bulletin of the*  
947 *American Meteorological Society*, 94, 1339-1360, [https://doi.org/10.1175/BAMS-D-](https://doi.org/10.1175/BAMS-D-12-00121.1)  
948 [12-00121.1](https://doi.org/10.1175/BAMS-D-12-00121.1), 2013.

949 Jickells, T. D., An, Z. S., Andersen, K. K., Baker, A. R., Bergametti, G., Brooks, N., Cao,  
950 J. J., Boyd, P. W., Duce, R. A., Hunter, K. A., Kawahata, H., Kubilay, N., laRoche, J.,  
951 Liss, P. S., Mahowald, N., Prospero, J. M., Ridgwell, A. J., Tegen, I., and Torres, R.:  
952 Global Iron Connections Between Desert Dust, Ocean Biogeochemistry, and  
953 Climate, 308, 67-71, <https://doi.org/10.1126/science.1105959> %J Science, 2005.

954 Kohfeld, K. E., and Harrison, S. P.: DIRTMAP: the geological record of dust, *Earth-*  
955 *Science Reviews*, 54, 81-114, [https://doi.org/10.1016/S0012-8252\(01\)00042-3](https://doi.org/10.1016/S0012-8252(01)00042-3), 2001.

956 Lin, Z. H., Levy, J. K., Lei, H., and Bell, M. L.: Advances in Disaster Modeling,  
957 Simulation and Visualization for Sandstorm Risk Management in North China,  
958 *Remote Sens-Basel*, 4, 1337-1354, <https://doi.org/10.3390/Rs4051337>, 2012.

959 Liu, X., Easter, R. C., Ghan, S. J., Zaveri, R., Rasch, P., Shi, X., Lamarque, J. F.,  
960 Gettelman, A., Morrison, H., Vitt, F., Conley, A., Park, S., Neale, R., Hannay, C.,  
961 Ekman, A. M. L., Hess, P., Mahowald, N., Collins, W., Iacono, M. J., Bretherton, C.  
962 S., Flanner, M. G., and Mitchell, D.: Toward a minimal representation of aerosols in  
963 climate models: description and evaluation in the Community Atmosphere Model  
964 CAM5, *Geosci. Model Dev.*, 5, 709-739, <https://doi.org/10.5194/gmd-5-709-2012>,

965 2012a.

966 [Luo, C., Mahowald, N. M., and del Corral, J.: Sensitivity study of meteorological](#)  
967 [parameters on mineral aerosol mobilization, transport, and distribution, 108,](#)  
968 [10.1029/2003jd003483, 2003.](#)

969 Liu, X., Shi, X., Zhang, K., Jensen, E. J., Gettelman, A., Barahona, D., Nenes, A., and  
970 Lawson, P.: Sensitivity studies of dust ice nuclei effect on cirrus clouds with the  
971 Community Atmosphere Model CAM5, *Atmos. Chem. Phys.*, 12, 12061-12079,  
972 <https://doi.org/10.5194/acp-12-12061-2012>, 2012b.

973 Maenhaut, W., Fernández-Jiménez, M. T., Rajta, I., Dubtsov, S., Meixner, F. X., Andreae,  
974 M. O., Torr, S., Hargrove, J. W., Chimanga, P., and Mlambo, J.: Long-term aerosol  
975 composition measurements and source apportionment at Rukomechi, Zimbabwe,  
976 *Journal of Aerosol Science*, 31, 228-229, [https://doi.org/10.1016/S0021-](https://doi.org/10.1016/S0021-8502(00)90237-4)  
977 [8502\(00\)90237-4](https://doi.org/10.1016/S0021-8502(00)90237-4), 2000a.

978 Maenhaut, W., Fernández-Jiménez, M. T., Vanderzalm, J. L., Hooper, B., Hooper, M. A.,  
979 and Tapper, N. J.: Aerosol composition at Jabiru, Australia, and impact of biomass  
980 burning, *Journal of Aerosol Science*, 31, 745-746, [https://doi.org/10.1016/S0021-](https://doi.org/10.1016/S0021-8502(00)90755-9)  
981 [8502\(00\)90755-9](https://doi.org/10.1016/S0021-8502(00)90755-9), 2000b.

982 Mahowald, N., Kohfeld, K., Hansson, M., Balkanski, Y., Harrison, S. P., Prentice, I. C.,  
983 Schulz, M., and Rodhe, H.: Dust sources and deposition during the last glacial  
984 maximum and current climate: A comparison of model results with paleodata from  
985 ice cores and marine sediments, 104, 15895-15916,  
986 <https://doi.org/10.1029/1999jd900084>, 1999.

987 Mahowald, N., Ward, D. S., Kloster, S., Flanner, M. G., Heald, C. L., Heavens, N. G.,  
988 Hess, P. G., Lamarque, J. F., and Chuang, P. Y.: Aerosol Impacts on Climate and  
989 Biogeochemistry, *Annu Rev Env Resour*, 36, 45-74, [https://doi.org/10.1146/annurev-](https://doi.org/10.1146/annurev-environ-042009-094507)  
990 [environ-042009-094507](https://doi.org/10.1146/annurev-environ-042009-094507), 2011.

991 Mahowald, N. M., Engelstaedter, S., Luo, C., Sealy, A., Artaxo, P., Benitez-Nelson, C.,  
992 Bonnet, S., Chen, Y., Chuang, P. Y., Cohen, D. D., Dulac, F., Herut, B., Johansen, A.  
993 M., Kubilay, N., Losno, R., Maenhaut, W., Paytan, A., Prospero, J. M., Shank, L. M.,  
994 and Siefert, R. L.: Atmospheric Iron Deposition: Global Distribution, Variability, and  
995 Human Perturbations, 1, 245-278,  
996 <https://doi.org/10.1146/annurev.marine.010908.163727>, 2009.

997 Marticorena, B., and Bergametti, G.: Modeling the Atmospheric Dust Cycle .1. Design of  
998 a Soil-Derived Dust Emission Scheme, *J Geophys Res-Atmos*, 100, 16415-16430,  
999 1995.

1000 Martin, G. M., Bellouin, N., Collins, W. J., Culverwell, I. D., Halloran, P. R., Hardiman,  
1001 S. C., Hinton, T. J., Jones, C. D., McDonald, R. E., McLaren, A. J., O'Connor, F. M.,



1002 Roberts, M. J., Rodriguez, J. M., Woodward, S., Best, M. J., Brooks, M. E., Brown,  
1003 A. R., Butchart, N., Dearden, C., Derbyshire, S. H., Dharssi, I., Doutriaux-Boucher,  
1004 M., Edwards, J. M., Falloon, P. D., Gedney, N., Gray, L. J., Hewitt, H. T., Hobson,  
1005 M., Huddleston, M. R., Hughes, J., Ineson, S., Ingram, W. J., James, P. M., Johns, T.  
1006 C., Johnson, C. E., Jones, A., Jones, C. P., Joshi, M. M., Keen, A. B., Liddicoat, S.,  
1007 Lock, A. P., Maidens, A. V., Manners, J. C., Milton, S. F., Rae, J. G. L., Ridley, J. K.,  
1008 Sellar, A., Senior, C. A., Totterdell, I. J., Verhoef, A., Vidale, P. L., and Wiltshire, A.:  
1009 The HadGEM2 family of Met Office Unified Model climate configurations, *Geosci.*  
1010 *Model Dev.*, 4, 723-757, <https://doi.org/10.5194/gmd-4-723-2011>, 2011.

1011 Miller, R. L., Cakmur, R. V., Perlwitz, J., Geogdzhayev, I. V., Ginoux, P., Koch, D.,  
1012 Kohfeld, K. E., Prigent, C., Ruedy, R., Schmidt, G. A., and Tegen, I.: Mineral dust  
1013 aerosols in the NASA Goddard Institute for Space Sciences ModelE atmospheric  
1014 general circulation model, *Journal of Geophysical Research: Atmospheres*, 111,  
1015 <https://doi.org/10.1029/2005JD005796>, 2006.

1016 Nyanganyura, D., Maenhaut, W., Mathuthu, M., Makarau, A., and Meixner, F. X.: The  
1017 chemical composition of tropospheric aerosols and their contributing sources to a  
1018 continental background site in northern Zimbabwe from 1994 to 2000, *Atmos*  
1019 *Environ*, 41, 2644-2659, <https://doi.org/10.1016/j.atmosenv.2006.11.015>, 2007.

1020 Prospero J M.: The Atmospheric transport of particles to the Ocean, in *Particle Flux in*  
1021 *the Ocean*, edited by Ittekkot V, Schäfer P, Honjo S, .and Depetris P J, SCOPE  
1022 Report 57, John Wiley & Sons, Chichester, 19-52, 1996.

1023 Prospero, J. M., Ginoux, P., Torres, O., Nicholson, S. E., and Gill, T. E.:  
1024 ENVIRONMENTAL CHARACTERIZATION OF GLOBAL SOURCES OF  
1025 ATMOSPHERIC SOIL DUST IDENTIFIED WITH THE NIMBUS 7 TOTAL  
1026 OZONE MAPPING SPECTROMETER (TOMS) ABSORBING AEROSOL  
1027 PRODUCT, 40, 2-1-2-31, <https://doi.org/10.1029/2000rg000095>, 2002.

1028 Pu, B., and Ginoux, P.: How reliable are CMIP5 models in simulating dust optical depth?,  
1029 *Atmos. Chem. Phys. Discuss.*, 2018, 1-60, [10.5194/acp-2018-242](https://doi.org/10.5194/acp-2018-242), 2018.

1030 Rahimi, S., Liu, X., Wu, C., Lau, W. K., Brown, H., Wu, M., and Qian, Y.: Quantifying  
1031 snow darkening and atmospheric radiative effects of black carbon and dust on the  
1032 South Asian monsoon and hydrological cycle: experiments using variable-resolution  
1033 CESM, *Atmos. Chem. Phys.*, 19, 12025-12049, [https://doi.org/10.5194/acp-19-](https://doi.org/10.5194/acp-19-12025-2019)  
1034 [12025-2019](https://doi.org/10.5194/acp-19-12025-2019), 2019.

1035 Randles, C. A., Silva, A. M. d., Buchard, V., Colarco, P. R., Darmenov, A., Govindaraju,  
1036 R., Smirnov, A., Holben, B., Ferrare, R., Hair, J., Shinozuka, Y., and Flynn, C. J.:  
1037 The MERRA-2 Aerosol Reanalysis, 1980 Onward. Part I: System Description and  
1038 Data Assimilation Evaluation, 30, 6823-6850, <https://doi.org/10.1175/jcli-d-16->

1039 0609.1, 2017.

1040 Rotstayn, L. D., Jeffrey, S. J., Collier, M. A., Dravitzki, S. M., Hirst, A. C., Syktus, J. I.,  
1041 and Wong, K. K.: Aerosol- and greenhouse gas-induced changes in summer rainfall  
1042 and circulation in the Australasian region: a study using single-forcing climate  
1043 simulations, *Atmos. Chem. Phys.*, 12, 6377-6404, [https://doi.org/10.5194/acp-12-](https://doi.org/10.5194/acp-12-6377-2012)  
1044 [6377-2012](https://doi.org/10.5194/acp-12-6377-2012), 2012.

1045 Ryder, C. L., Marengo, F., Brooke, J. K., Estelles, V., Cotton, R., Formenti, P., McQuaid,  
1046 J. B., Price, H. C., Liu, D., Ausset, P., Rosenberg, P. D., Taylor, J. W., Choularton, T.,  
1047 Bower, K., Coe, H., Gallagher, M., Crosier, J., Lloyd, G., Highwood, E. J., and  
1048 Murray, B. J.: Coarse-mode mineral dust size distributions, composition and optical  
1049 properties from AER-D aircraft measurements over the tropical eastern Atlantic,  
1050 *Atmos. Chem. Phys.*, 18, 17225-17257, <https://doi.org/10.5194/acp-18-17225-2018>,  
1051 2018.

1052 Sakamoto, T. T., Komuro, Y., Nishimura, T., Ishii, M., Tatebe, H., Shiogama, H.,  
1053 Hasegawa, A., Toyoda, T., Mori, M., Suzuki, T., Imada, Y., Nozawa, T., Takata, K.,  
1054 Mochizuki, T., Ogochi, K., Emori, S., Hasumi, H., and Kimoto, M.: MIROC4h - A  
1055 New High-Resolution Atmosphere-Ocean Coupled General Circulation Model,  
1056 *Journal of the Meteorological Society of Japan. Ser. II*, 90, 325-359,  
1057 <https://doi.org/10.2151/jmsj.2012-301>, 2012.

1058 Schmidt, G. A., Kelley, M., Nazarenko, L., Ruedy, R., Russell, G. L., Aleinov, I., Bauer,  
1059 M., Bauer, S. E., Bhat, M. K., Bleck, R., Canuto, V., Chen, Y.-H., Cheng, Y., Clune,  
1060 T. L., Del Genio, A., de Fainchtein, R., Faluvegi, G., Hansen, J. E., Healy, R. J.,  
1061 Kiang, N. Y., Koch, D., Lacis, A. A., LeGrande, A. N., Lerner, J., Lo, K. K.,  
1062 Matthews, E. E., Menon, S., Miller, R. L., Oinas, V., Oloso, A. O., Perlwitz, J. P.,  
1063 Puma, M. J., Putman, W. M., Rind, D., Romanou, A., Sato, M., Shindell, D. T., Sun,  
1064 S., Syed, R. A., Tausnev, N., Tsigaridis, K., Unger, N., Voulgarakis, A., Yao, M.-S.,  
1065 and Zhang, J.: Configuration and assessment of the GISS ModelE2 contributions to  
1066 the CMIP5 archive, *Journal of Advances in Modeling Earth Systems*, 6, 141-184,  
1067 <https://doi.org/10.1002/2013MS000265>, 2014.

1068 Shao, Y.: *Physics and modelling of wind erosion*, Springer, Berlin, Germany, 2008.

1069 Shao, Y., Leys, J. F., McTainsh, G. H., and Tews, K.: Numerical simulation of the  
1070 October 2002 dust event in Australia, 112, [10.1029/2006jd007767](https://doi.org/10.1029/2006jd007767), 2007.

1071 Shao, Y., Raupach, M. R., & Leys, J. F. (1996). A model for predicting aeolian sand drift  
1072 and dust entrainment on scales from paddock to region, *Australian Journal of Soil*  
1073 *Research*, 34(3), 309-342, <https://doi.org/10.1071/SR9960309>, 1996.

1074 Shao, Y. P., Wyrwoll, K. H., Chappell, A., Huang, J. P., Lin, Z. H., McTainsh, G. H.,  
1075 Mikami, M., Tanaka, T. Y., Wang, X. L., and Yoon, S.: Dust cycle: An emerging core

1076 theme in Earth system science, *Aeolian Res*, 2, 181-204,  
1077 <https://doi.org/10.1016/j.aeolia.2011.02.001>, 2011.

1078 Takemura, T., Okamoto, H., Maruyama, Y., Numaguti, A., Higurashi, A., and Nakajima,  
1079 T.: Global three-dimensional simulation of aerosol optical thickness distribution of  
1080 various origins, *Journal of Geophysical Research: Atmospheres*, 105, 17853-17873,  
1081 <https://doi.org/10.1029/2000JD900265>, 2000.

1082 Takemura, T., Egashira, M., Matsuzawa, K., Ichijo, H., O'Ishi, R., and Abe-Ouchi, A.: A  
1083 simulation of the global distribution and radiative forcing of soil dust aerosols at the  
1084 Last Glacial Maximum, *Atmos. Chem. Phys.*, 9, 3061-3073,  
1085 <https://doi.org/10.5194/acp-9-3061-2009>, 2009.

1086 Tanaka, T. Y., and Chiba, M.: Global Simulation of Dust Aerosol with a Chemical  
1087 Transport Model, MASINGAR, *Journal of the Meteorological Society of Japan. Ser.*  
1088 *II*, 83A, 255-278, 10.2151/jmsj.83A.255, 2005.

1089 Tanaka, T. Y., and Chiba, M.: A numerical study of the contributions of dust source  
1090 regions to the global dust budget, *Global Planet Change*, 52, 88-104,  
1091 <https://doi.org/10.1016/j.gloplacha.2006.02.002>, 2006.

1092 [Taylor, K. E., Stouffer, R. J., and Meehl, G. A.: A summary of the CMIP5 experiment](#)  
1093 [design. PCDMI Rep., 33 pp. 2009. \[Available online at](#)  
1094 [\[https://pcmdi.llnl.gov/mips/cmip5/docs/Taylor\\\_CMIP5\\\_22Jan11\\\_marked.pdf?id=73\]\(https://pcmdi.llnl.gov/mips/cmip5/docs/Taylor\_CMIP5\_22Jan11\_marked.pdf?id=73\),](#)  
1095 [accessed on June 25, 2020.\]](#)

1096 [Taylor, K. E., Stouffer, R. J., and Meehl, G. A.: An Overview of CMIP5 and the](#)  
1097 [Experiment Design. \*Bulletin of the American Meteorological Society\*, 93, 485-498,](#)  
1098 [10.1175/BAMS-D-11-00094.1, 2012.](#)

1099 [Tegen, I., Harrison, S. P., Kohfeld, K., Prentice, I. C., Coe, M., and Heimann, M.: Impact](#)  
1100 [of vegetation and preferential source areas on global dust aerosol: Results from a](#)  
1101 [model study. 107, AAC 14-11-AAC 14-27, 10.1029/2001jd000963, 2002.](#)

1102 [Textor, C., Schulz, M., Guibert, S., Kinne, S., Balkanski, Y., Bauer, S., Berntsen, T.,](#)  
1103 [Berglen, T., Boucher, O., Chin, M., Dentener, F., Diehl, T., Easter, R., Feichter, H.,](#)  
1104 [Fillmore, D., Ghan, S., Ginoux, P., Gong, S., Grini, A., Hendricks, J., Horowitz, L.,](#)  
1105 [Huang, P., Isaksen, I., Iversen, I., Kloster, S., Koch, D., Kirkevåg, A., Kristjansson, J.](#)  
1106 [E., Krol, M., Lauer, A., Lamarque, J. F., Liu, X., Montanaro, V., Myhre, G., Penner,](#)  
1107 [J., Pitari, G., Reddy, S., Seland, Ø., Stier, P., Takemura, T., and Tie, X.: Analysis and](#)  
1108 [quantification of the diversities of aerosol life cycles within AeroCom, \*Atmos. Chem.\*](#)  
1109 [\*Phys.\*, 6, 1777-1813, 10.5194/acp-6-1777-2006, 2006.](#)

1110 [Textor, C., Schulz, M., Guibert, S., Kinne, S., Balkanski, Y., Bauer, S., Berntsen, T.,](#)  
1111 [Berglen, T., Boucher, O., Chin, M., Dentener, F., Diehl, T., Feichter, J., Fillmore, D.,](#)  
1112 [Ginoux, P., Gong, S., Grini, A., Hendricks, J., Horowitz, L., Huang, P., Isaksen, I. S.](#)

1113 [A., Iversen, T., Kloster, S., Koch, D., Kirkevåg, A., Kristjansson, J. E., Krol, M.,](#)  
 1114 [Lauer, A., Lamarque, J. F., Liu, X., Montanaro, V., Myhre, G., Penner, J. E., Pitari,](#)  
 1115 [G., Reddy, M. S., Seland, Ø., Stier, P., Takemura, T., and Tie, X.: The effect of](#)  
 1116 [harmonized emissions on aerosol properties in global models – an AeroCom](#)  
 1117 [experiment, \*Atmos. Chem. Phys.\*, 7, 4489-4501, 10.5194/acp-7-4489-2007, 2007.](#)  
 1118 [Todd, M. C., Karam, D. B., Cavazos, C., Bouet, C., Heinold, B., Baldasano, J. M.,](#)  
 1119 [Cautenet, G., Koren, I., Perez, C., Solmon, F., Tegen, I., Tulet, P., Washington, R.,](#)  
 1120 [and Zakey, A.: Quantifying uncertainty in estimates of mineral dust flux: An](#)  
 1121 [intercomparison of model performance over the Bodele Depression, northern Chad,](#)  
 1122 [J Geophys Res-Atmos, 113, D24107, 10.1029/2008jd010476, 2008.](#)  
 1123 [Uno, I., Wang, Z., Chiba, M., Chun, Y. S., Gong, S. L., Hara, Y., Jung, E., Lee, S. S., Liu,](#)  
 1124 [M., Mikami, M., Music, S., Nickovic, S., Satake, S., Shao, Y., Song, Z., Sugimoto,](#)  
 1125 [N., Tanaka, T., and Westphal, D. L.: Dust model intercomparison \(DMIP\) study](#)  
 1126 [over Asia: Overview, J Geophys Res-Atmos, 111, D12213, 10.1029/2005jd006575,](#)  
 1127 [2006.](#)  
 1128 Vanderzalm, J. L., Hooper, M. A., Ryan, B., Maenhaut, W., Martin, P., Rayment, P. R.,  
 1129 and Hooper, B. M.: Impact of seasonal biomass burning on air quality in the "Top  
 1130 End" of regional Northern Australia, *Clean Air and Environmental Quality*, 37(3),  
 1131 28–34, 2003.  
 1132 von Salzen, K., Scinocca, J. F., McFarlane, N. A., Li, J., Cole, J. N. S., Plummer, D.,  
 1133 Verseghy, D., Reader, M. C., Ma, X., Lazare, M., and Solheim, L.: The Canadian  
 1134 Fourth Generation Atmospheric Global Climate Model (CanAM4). Part I:  
 1135 Representation of Physical Processes, *Atmosphere-Ocean*, 51, 104-125,  
 1136 <https://doi.org/10.1080/07055900.2012.755610>, 2013.  
 1137 Watanabe, M., Suzuki, T., O'ishi, R., Komuro, Y., Watanabe, S., Emori, S., Takemura, T.,  
 1138 Chikira, M., Ogura, T., Sekiguchi, M., Takata, K., Yamazaki, D., Yokohata, T.,  
 1139 Nozawa, T., Hasumi, H., Tatebe, H., and Kimoto, M.: Improved Climate Simulation  
 1140 by MIROC5: Mean States, Variability, and Climate Sensitivity, *J Climate*, 23, 6312-  
 1141 6335, <https://doi.org/10.1175/2010jcli3679.1>, 2010.  
 1142 Watanabe, S., Hajima, T., Sudo, K., Nagashima, T., Takemura, T., Okajima, H., Nozawa,  
 1143 T., Kawase, H., Abe, M., Yokohata, T., Ise, T., Sato, H., Kato, E., Takata, K., Emori,  
 1144 S., and Kawamiya, M.: MIROC-ESM 2010: model description and basic results of  
 1145 CMIP5-20c3m experiments, *Geosci. Model Dev.*, 4, 845-872,  
 1146 <https://doi.org/10.5194/gmd-4-845-2011>, 2011.  
 1147 Woodward, S.: Modeling the atmospheric life cycle and radiative impact of mineral dust  
 1148 in the Hadley Centre climate model, *Journal of Geophysical Research: Atmospheres*,  
 1149 106, 18155-18166, <https://doi.org/10.1029/2000JD900795>, 2001.

1150 Woodward, S.: Mineral dust in HadGEM2, Hadley Centre tech. Note 87. Met Office,  
1151 Exeter, Devon, UK, 2011.

1152 Wu, C., and Lin, Z.: Uncertainty in Dust Budget over East Asia Simulated by WRF/Chem  
1153 with Six Different Dust Emission Schemes, *Atmospheric and Oceanic Science*  
1154 *Letters*, 6, 428-433, <https://doi.org/10.3878/j.issn.1674-2834.13.0045>, 2013.

1155 Wu, C., Lin, Z., He, J., Zhang, M., Liu, X., Zhang, R., and Brown, H.: A process-oriented  
1156 evaluation of dust emission parameterizations in CESM: Simulation of a typical  
1157 severe dust storm in East Asia, *Journal of Advances in Modeling Earth Systems*, 8,  
1158 1432-1452, <https://doi.org/10.1002/2016MS000723>, 2016.

1159 Wu, C., Lin, Z., Liu, X., Li, Y., Lu, Z., and Wu, M.: Can Climate Models Reproduce the  
1160 Decadal Change of Dust Aerosol in East Asia?, 45, 9953-9962,  
1161 <https://doi.org/10.1029/2018gl079376>, 2018a.

1162 Wu, C., Liu, X., Lin, Z., Rahimi-Esfarjani, S. R., and Lu, Z.: Impacts of absorbing  
1163 aerosol deposition on snowpack and hydrologic cycle in the Rocky Mountain region  
1164 based on variable-resolution CESM (VR-CESM) simulations, *Atmos. Chem. Phys.*,  
1165 18, 511-533, <https://doi.org/10.5194/acp-18-511-2018>, 2018b.

1166 Wu, M., Liu, X., Yang, K., Luo, T., Wang, Z., Wu, C., Zhang, K., Yu, H., and Darmanov,  
1167 A.: Modeling Dust in East Asia by CESM and Sources of Biases, 124, 8043-8064,  
1168 <https://doi.org/10.1029/2019jd030799>, 2019.

1169 Yue, X., Wang, H. J., Wang, Z. F., and Fan, K.: Simulation of dust aerosol radiative  
1170 feedback using the Global Transport Model of Dust: 1. Dust cycle and validation, *J*  
1171 *Geophys Res-Atmos*, 114, Artn D10202, <https://doi.org/10.1029/2008jd010995>,  
1172 2009.

1173 Yue, X., Wang, H., Liao, H., and Fan, K.: Simulation of dust aerosol radiative feedback  
1174 using the GMOD: 2. Dust-climate interactions, 115,  
1175 <https://doi.org/10.1029/2009jd012063>, 2010.

1176 Yukimoto, S., Adachi, Y., Hosaka, M., Sakami, T., Yoshimura, H., Hirabara, M., Tanaka,  
1177 T. Y., Shindo, E., Tsujino, H., Deushi, M., Mizuta, R., Yabu, S., Obata, A., Nakano,  
1178 H., Koshiro, T., Ose, T., and Kitoh, A.: A New Global Climate Model of the  
1179 Meteorological Research Institute: MRI-CGCM3—Model Description and Basic  
1180 Performance, *Journal of the Meteorological Society of Japan. Ser. II*, 90A, 23-64,  
1181 <https://doi.org/10.2151/jmsj.2012-A02>, 2012.

1182 Yukimoto, S., Yoshimura, H., Hosaka, M., Sakami, T., Tsujino, H., Hirabara, M., et al.:  
1183 Meteorological Research Institute-Earth System Model v1 (MRI-ESM 1)—Model  
1184 description, Technical Report of MRI, Ibaraki, Japan, 2011.

1185 [Yumimoto, K., Uno, I., Sugimoto, N., Shimizu, A., and Satake, S.: Adjoint inverse](#)  
1186 [modeling of dust emission and transport over East Asia, 34, 10.1029/2006gl028551,](#)

1187 [2007](#).  
1188 Zender, C. S., Bian, H. S., and Newman, D.: Mineral Dust Entrainment and Deposition  
1189 (DEAD) model: Description and 1990s dust climatology, J Geophys Res-Atmos,  
1190 108, 4416, <https://doi.org/10.1029/2002jd002775>, 2003.  
1191

1193 **Table 1.** CMIP5 model used in this study. For comparison with CMIP5 models, MERRA-2 reanalysis is also included.

No.	Models <sup>a</sup>	Resolution	Ensemble number	Dust size (in diameter)	Vegetation cover for dust emission	Dust emission scheme	Model reference
1	ACCESS1-0	1.3° × 1.9°	3	6 bins: 0.0632-0.2-0.632-2-6.32-20-63.2 μm	Prescribed	Woodward (2001, 2011)	Bi et al. (2013) Dix et al. (2013)
2	<a href="#">HadGEM2-CC</a>	<a href="#">1.3° × 1.9°</a>	<a href="#">3</a>	<a href="#">6 bins: 0.0632-0.2-0.632-2-6.32-20-63.2 μm</a>	<a href="#">Prognostic</a>	<a href="#">Woodward (2001, 2011)</a>	<a href="#">Collins et al. (2011)</a> <a href="#">Martin et al. (2011)</a>
3	<a href="#">HadGEM2-ES</a>	<a href="#">1.3° × 1.9°</a>	<a href="#">4</a>	<a href="#">As HadGEM2-CC</a>	<a href="#">Prognostic</a>	<a href="#">Woodward (2001, 2011)</a>	<a href="#">Collins et al. (2011)</a> <a href="#">Martin et al. (2011)</a>
4	<a href="#">GFDL-CM3</a>	<a href="#">2° × 2.5°</a>	<a href="#">5</a>	<a href="#">5 bins: 0.2-2-3.6-6-12-20 μm</a>	<a href="#">Prescribed</a>	<a href="#">Ginoux et al. (2001)</a>	<a href="#">Delworth et al. (2006)</a> <a href="#">Donner et al. (2011)</a>
5	<a href="#">MIROC4h</a>	<a href="#">0.56° × 0.56°</a>	<a href="#">1</a>	<a href="#">10 bins: 0.2-0.32-0.5-0.8-1.26-2-3.16-5.02-7.96-12.62-20 μm</a>	<a href="#">Prescribed</a>	<a href="#">Takemura et al. (2000)</a>	<a href="#">Sakamoto et al. (2012)</a>
6	<a href="#">MIROC5</a>	<a href="#">1.4° × 1.4°</a>	<a href="#">5</a>	<a href="#">6 bins: 0.2-0.43-0.93-2-4.3-9.3-20 μm</a>	<a href="#">Prescribed</a>	<a href="#">Takemura et al. (2000, 2009)</a>	<a href="#">Watanabe et al. (2010)</a>
7	<a href="#">MIROC-ESM</a>	<a href="#">2.8° × 2.8°</a>	<a href="#">1</a>	<a href="#">As MIROC4h</a>	<a href="#">Prognostic</a>	<a href="#">Takemura et al. (2000, 2009)</a>	<a href="#">Watanabe et al. (2011)</a>
8	<a href="#">MIROC-ESM-CHEM</a>	<a href="#">2.8° × 2.8°</a>	<a href="#">3</a>	<a href="#">As MIROC4h</a>	<a href="#">Prognostic</a>	<a href="#">Takemura et al. (2000, 2009)</a>	<a href="#">Watanabe et al. (2011)</a>
9	<a href="#">MRI-CGCM3</a>	<a href="#">1.1° × 1.1°</a>	<a href="#">5</a>	<a href="#">6 bins: 0.2-0.43-0.93-2-4.3-9.3-20 μm</a>	<a href="#">Prescribed</a>	<a href="#">Shao et al. (1996)</a> <a href="#">Tanaka and Chiba (2005, 2006)</a>	<a href="#">Yukimoto et al. (2011, 2012)</a>
10	<a href="#">MRI-ESM1</a>	<a href="#">1.1° × 1.1°</a>	<a href="#">1</a>	<a href="#">6 bins: 0.2-0.43-0.93-2-4.3-9.3-20 μm</a>	<a href="#">Prescribed</a>	<a href="#">Shao et al. (1996)</a> <a href="#">Tanaka and Chiba (2005, 2006)</a>	<a href="#">Yukimoto et al. (2011, 2012)</a> <a href="#">Adachi et al. (2013)</a>
11	CanESM2	2.8° × 2.8°	5	2 modes: MMD=0.78 μm (σ=2) and 3.8 μm (σ=2.15) <sup>b</sup>	Prescribed	Martcorena and Bergametti (1995)	Arora et al. (2011) von Salzen et al. (2013)

带格式表格

带格式表格

<del>123</del>	CESM1-CAM5	0.9° × 1.25°	2	2 modes: 0.1-1-10 μm <sup>c</sup>	Prescribed	Zender et al. (2003)	Hurrell et al. (2013)
<del>134</del>	CSIRO-Mk3-6-0	1.9° × 1.9°	10	4 bins: 0.2-2-4-6-12 μm	Prescribed	Ginoux et al. (2001, 2004)	Rotstaysn et al. (2012)
<del>5</del>	<del>GFDL-CM3</del>	<del>2° × 2.5°</del>	<del>5</del>	<del>5 bins: 0.2-2-3.6-6- 12-20 μm</del>	<del>Prognostic</del>	<del>Ginoux et al. (2001)</del>	<del>Delworth et al. (2006) Donner et al. (2011)</del>
<del>146</del>	GISS-E2-H	2° × 2.5°	12	4 bins: <2, 2-4-8-16 μm	Prescribed <sup>d</sup>	Cakmur et al. (2006) Miller et al. (2006)	Schmidt et al. (2014)
<del>157</del>	GISS-E2-R	2° × 2.5°	12	4 bins: <2, 2-4-8-16 μm	Prescribed <sup>d</sup>	Cakmur et al. (2006) Miller et al. (2006)	Schmidt et al. (2014)
<del>8</del>	HadGEM2-CC	1.3° × 1.9°	3	<del>6 bins: 0.0632-0.2- 0.632-2-6.32-20-63.2 μm</del>	<del>Prognostic</del>	<del>Woodward (2001, 2011)</del>	<del>Collins et al. (2011) Martin et al. (2011)</del>
<del>9</del>	HadGEM2-ES	1.3° × 1.9°	4	As HadGEM2-CC	Prognostic	Woodward (2001, 2011)	Collins et al. (2011) Martin et al. (2011)
<del>10</del>	MIROC4h	0.56° × 0.56°	1	<del>10 bins: 0.2-0.32-0.5- 0.8-1.26-2-3.16-5.02- 7.96-12.62-20 μm</del>	<del>Prescribed</del>	<del>Takemura et al. (2000)</del>	<del>Sakamoto et al. (2012)</del>
<del>11</del>	MIROC5	1.4° × 1.4°	5	<del>6 bins: 0.2-0.43-0.93- 2-4.3-9.3-20 μm</del>	<del>Prescribed</del>	<del>Takemura et al. (2000, 2009)</del>	<del>Watanabe et al. (2010)</del>
<del>12</del>	MIROC-ESM	2.8° × 2.8°	1	As MIROC4h	Prognostic	Takemura et al. (2000, 2009)	Watanabe et al. (2011)
<del>13</del>	MIROC-ESM- CHEM	2.8° × 2.8°	3	As MIROC4h	Prognostic	Takemura et al. (2000, 2009)	Watanabe et al. (2011)
<del>14</del>	MRI-CGCM3	1.1° × 1.1°	5	<del>6 bins: 0.2-0.43-0.93- 2-4.3-9.3-20 μm</del>	<del>Prescribed</del>	<del>Shao et al. (1996) Tanaka and Chiba (2005, 2006)</del>	<del>Yukimoto et al. (2011, 2012)</del>
<del>15</del>	MRI-ESM1	1.1° × 1.1°	1	<del>6 bins: 0.2-0.43-0.93- 2-4.3-9.3-20 μm</del>	<del>Prescribed</del>	<del>Shao et al. (1996) Tanaka and Chiba (2005, 2006)</del>	<del>Yukimoto et al. (2011, 2012) Adachi et al. (2013)</del>
16	MERRA-2	0.5° × 0.625°	1	5 bins: 0.2-2-3.6-6- 12-20 μm	Prescribed	Ginoux et al. (2001)	Randles et al. (2017) Buchard et al. (2017)



1194 <sup>a</sup>: Expansions of acronyms: ACCESS1-0, Australian Community Climate and Earth-System Simulator version 1.0; CanESM2, Second Generation Canadian Earth  
1195 System Model; CESM1-CAM5, Community Earth System Model version 1-Community Atmosphere Model version 5; CSIRO-Mk3-6-0, Commonwealth Scientific  
1196 and Industrial Research Organization Mark 3.6.0; GFDL-CM3, Geophysical Fluid Dynamics Laboratory Climate Model version 3; GISS-E2-H, Goddard Institute for  
1197 Space Studies Model E2 coupled with HYCOM (Hybrid Coordinate Ocean Model); GISS-E2-R, Goddard Institute for Space Studies Model E2 coupled with the  
1198 Russell ocean model; HadGEM2-CC, Hadley Centre Global Environment Model version 2 with Carbon Cycle configuration; HadGEM2-ES, Hadley Centre Global  
1199 Environment Model version 2 with Earth System configuration; MIROC4h, Model for Interdisciplinary Research on Climate version 4 (high resolution); MIROC5,  
1200 Model for Interdisciplinary Research on Climate version 5; MIROC-ESM, Model for Interdisciplinary Research on Climate-Earth System Model; MIROC-ESM-  
1201 CHEM, Model for Interdisciplinary Research on Climate-Earth System Model with Chemistry Coupled; MRI-CGCM3, Meteorological Research Institute Coupled  
1202 Atmosphere–Ocean General Circulation Model version 3; MRI-ESM1, Meteorological Research Institute Earth System Model version 1.  
1203 <sup>b</sup>: MMD is the abbreviation of mass median diameter and  $\sigma$  is geometric standard deviation.  
1204 <sup>c</sup>: Dust emission is calculated in the size range of 0.1-1 and 1-10  $\mu\text{m}$  for accumulation and coarse modes, respectively.  
1205 <sup>d</sup>: [Surface roughness that is comparable to vegetation data is used for dust emission calculation \(Miller et al., 2006\).](#)

1206 **Table 2.** The location of observational stations for ~~(a)~~ surface dust concentration ~~and~~  
 1207 ~~(b)~~ fraction of wet deposition used in this study.

1208 (a)

No.	Name	Latitude	Longitude	Period
1	Miami	25.75°N	80.25°W	<u>Jan 1989 – Aug 1998</u>
2	Bermuda	32.27°N	64.87°W	<u>Mar 1989 – Jan 1998</u>
3	Barbados	13.17°N	59.43°W	<u>May 1984 – Jul 1998</u>
4	Izana Tenerife	28.3°N	16.5°W	<u>Jul 1987 – Jul 1998</u>
5	Mace Head	53.32°N	9.85°W	<u>Aug 1988 – Aug 1994</u>
6	Rukomechi	16°S	29.5°E	<u>Sep 1994 – Jan 2000</u>
7	Cheju	33.52°N	126.48°E	<u>Sep 1991 – Oct 1995</u>
8	Hedo	26.92°N	128.25°E	<u>Sep 1991 – Mar 1994</u>
9	Enewetak Atoll	11.33°N	162.33°E	<u>Feb 1981 – Jun 1987</u>
10	Nauru	0.53°N	166.95°E	<u>Mar 1983 – Oct 1987</u>
11	Midway Island	28.22°N	177.35°W	<u>Jan 1981 – Jan 1997</u>
12	Fanning Island	3.92°N	159.33°W	<u>Apr 1981 – Aug 1986</u>
13	Hawaii	21.33°N	157.7°W	<u>Jan 1981 – Jul 1995</u>
14	Jabirun	12.7°S	132.9°E	<u>May 1995 – Dec 1996</u>
15	Cape Grim	40.68°S	144.68°E	<u>Jan 1983 – Nov 1996</u>
16	New Caledonia	22.15°S	167°E	<u>Aug 1983 – Oct 1985</u>
17	Norfolk Island	29.08°S	167.98°E	<u>May 1983 – Feb 1997</u>
18	Funafuti	8.5°S	179.2°W	<u>Apr 1983 – Jul 1987</u>
19	American Samoa	14.25°S	170.58°W	<u>Mar 1983 – Jan 1996</u>
20	Cook Islands	21.25°S	159.75°W	<u>Mar 1983 – Jun 1994</u>
21	Palmer	64.77°S	64.05°W	<u>Apr 1990 – Oct 1996</u>
22	Mawson	67.6°S	62.5°E	<u>Jeb 1987 – Jan 1996</u>

1209

1210 (b)

No.	Name	Latitude	Longitude	No.	Name	Latitude	Longitude
1	Bermuda	32.27°N	64.87°W	6	New Zealand	34.55°S	172.75°E
2	Amsterdam Island	37.83°S	77.5°E	7	Midway	28.22°N	177.35°W
3	Cape Ferrat	43.68°N	7.33°E	8	Fanning	3.92°N	159.33°W
4	Enewetak Atoll	11.33°N	162.33°E	9	Greenland	65°N	44°W
5	Samoa	14.25°S	170.57°W	10	Coastal Antarctica	75.6°S	26.8°W

1211

1212

1213

1214

1215 **Table 3.** Global dust budgets in CMIP5 models. The models are classified into three  
 1216 groups according to the dust size range considered. Also included for comparison is  
 1217 MERRA-2 reanalysis.

Model	Size (diameter, $\mu\text{m}$ )	Emission <sup>a</sup> (Tg/yr)	Wet deposition <sup>b</sup> (Tg/yr)	Burden (Tg)	Life time (day)
ACCESS1-0	<u>0.06-63</u>	2218 (13%)	261 (12%)	8.1	1.3
<u>HadGEM2-CC</u>		<u>8186 (11%)</u>	<u>1521 (19%)</u>	<u>41.9</u>	<u>1.9</u>
<u>HadGEM2-ES</u>		<u>7972 (10%)</u>	<u>1429 (18%)</u>	<u>41.4</u>	<u>1.9</u>
<u>GFDL-CM3</u>	<u>0.2-20</u>	<u>1246 (10%)</u>	<u>210 (17%)</u>	<u>13.5</u>	<u>4.0</u>
<u>MIROC4h</u>		<u>735 (2.9%)</u>	<u>179 (24%)</u>	<u>2.5</u>	<u>1.4</u>
<u>MIROC5</u>		<u>2716 (6.1%)</u>	<u>668 (25%)</u>	<u>19.0</u>	<u>3.0</u>
<u>MIROC-ESM</u>		<u>3339 (5.2%)</u>	<u>540 (16%)</u>	<u>15.5</u>	<u>2.0</u>
<u>MIROC-ESM- CHEM</u>		<u>3598 (5.2%)</u>	<u>591 (16%)</u>	<u>16.7</u>	<u>2.0</u>
<u>MRI-CGCM3</u>		<u>2107 (5.9%)</u>	<u>819 (39%)</u>	<u>14.3</u>	<u>2.5</u>
<u>MRI-ESM1</u>		<u>2052 (6.1%)</u>	<u>801 (39%)</u>	<u>13.9</u>	<u>2.5</u>
CanESM2 <sup>c</sup>	<u>Median (0.78, 3.8)</u>	2964 (18%)	882 (30%)	35.8	4.4
CESM1-CAM5	<u>0.1 - 10</u>	3454 (2.0%)	1243 (36%)	24.9	2.6
CSIRO-Mk3-6-0	<u>0.2 - 12</u>	3698 (8.9%)	1024 (28%)	36.1	3.6
<u>GFDL-CM3</u>		<u>1246 (10%)</u>	<u>210 (17%)</u>	<u>13.5</u>	<u>4.0</u>
GISS-E2-H	<u>&lt;2 to 16</u>	1699 (8.2%)	641 (38%)	17.5	3.8
GISS-E2-R	<u>&lt;2 to 16</u>	1677 (8.2%)	625 (37%)	16.9	3.7
<u>HadGEM2-CC</u>		<u>8186 (11%)</u>	<u>1521 (19%)</u>	<u>41.9</u>	<u>1.9</u>
<u>HadGEM2-ES</u>		<u>7972 (10%)</u>	<u>1429 (18%)</u>	<u>41.4</u>	<u>1.9</u>
<u>MIROC4h</u>		<u>735 (2.9%)</u>	<u>179 (24%)</u>	<u>2.5</u>	<u>1.4</u>

带格式表格

带格式表格

MIROC5		2716 (6.1%)	668 (25%)	19.0	3.0
MIROC-ESM		3339 (5.2%)	540 (16%)	15.5	2.0
MIROC-ESM-CHEM		3598 (5.2%)	591 (16%)	16.7	2.0
MRI-CGCM3		2107 (5.9%)	819 (39%)	14.3	2.5
MRI-ESM1		2052 (6.1%)	801 (39%)	13.9	2.5
MERRA-2 <sup>cd</sup>	<u>0.2-20</u>	1620 (7.4%)	692 (38.6%)	20.3	4.1

1218 <sup>a</sup>: The global dust emission area fraction is given in parenthesis next to the global dust  
1219 emission. The dust emission area is defined as the region with the annual mean dust  
1220 emission flux larger than 1% of global mean annual dust emission flux.

1221 <sup>b</sup>: The ratio of wet deposition to total deposition is given in parenthesis next to wet  
1222 deposition.

1223 <sup>c</sup>: Using two modes, CanESM2 represents more than 97% of dust mass for particles  
1224 smaller than 16  $\mu\text{m}$  (in diameter). Therefore, CanESM2 is put into the third group.

1225 <sup>bd</sup>: The global dust deposition is 1692 Tg, which is larger than dust emission because  
1226 of no adjustment done with dust emission after aerosol assimilation (Section 2).

1227 **Table 4.** Dust emission amount (Tg) in nine dust source regions. The contribution of each source region to global total dust emission is given in  
 1228 the parenthesis next to dust emission amount.

No.	Models	Global	North Africa	Middle East	Central Asia	South Asia	East Asia	Australia	North America	South America	South Africa
1	ACCESS1-0	2218	1097 (49.5%)	356 (16.1%)	95 (4.3%)	159 (7.2%)	132 (6.0%)	254 (11.4%)	49 (2.2%)	46 (2.1%)	21 (1.0%)
<del>2</del>	<del>HadGEM2-CC</del>	<del>8186</del>	<del>3124 (38.2%)</del>	<del>593 (7.2%)</del>	<del>403 (4.9%)</del>	<del>826 (10.1%)</del>	<del>359 (4.4%)</del>	<del>2278 (27.8%)</del>	<del>264 (3.2%)</del>	<del>196 (2.4%)</del>	<del>142 (1.7%)</del>
3	HadGEM2-ES	7973	3221 (40.4%)	579 (7.3%)	418 (5.2%)	820 (10.3%)	321 (4.0%)	1988 (24.9%)	340 (4.3%)	144 (1.8%)	139 (1.7%)
4	GFDL-CM3	1246	749 (60.1%)	150 (12.1%)	68 (5.4%)	41 (3.3%)	113 (9.1%)	52 (4.2%)	5 (0.4%)	44 (3.6%)	19 (1.5%)
5	MIROC4h	735	437 (59.4%)	71 (9.7%)	81 (11.1%)	45 (6.1%)	64 (8.8%)	9 (1.2%)	0.1 (0.02%)	3 (0.5%)	24 (3.2%)
6	MIROC5	2716	1762 (64.9%)	269 (9.9%)	175 (6.5%)	96 (3.5%)	243 (8.9%)	26 (1.0%)	4 (0.2%)	79 (2.9%)	61 (2.2%)
7	MIROC-ESM	3339	2627 (78.7%)	244 (7.3%)	72 (2.2%)	30 (0.9%)	273 (8.2%)	0.6 (0.02%)	0.3 (0.008%)	89 (2.6%)	6 (0.2%)
8	MIROC-ESM-CHEM	3598	2719 (75.6%)	274 (7.6%)	84 (2.3%)	44 (1.2%)	362 (10.1%)	1 (0.03%)	0.4 (0.01%)	100 (2.8%)	13 (0.4%)
9	MRI-CGCM3	2107	1146 (54.4%)	258 (12.2%)	22 (1.1%)	174 (8.3%)	390 (18.5%)	55 (2.6%)	2 (0.09%)	49 (2.3%)	11 (0.5%)
10	MRI-ESM1	2052	1108 (54.0%)	246 (12.0%)	21 (1.0%)	167 (8.1%)	392 (19.1%)	57 (2.8%)	2 (0.09%)	48 (2.3%)	10 (0.5%)
<del>1</del>	CanESM2	2964	1053 (35.5%)	415 (14.0%)	323 (10.9%)	99 (3.3%)	151 (5.1%)	218 (7.3%)	133 (4.5%)	365 (12.3%)	96 (3.2%)
<del>1</del>	CESM1-	3454	1609 (46.6%)	698 (20.2%)	495 (14.3%)	122 (3.5%)	329 (9.5%)	38 (1.1%)	35 (1.0%)	26 (0.7%)	101 (2.9%)
<del>2</del>	CAM5	3698	1863 (50.4%)	555 (15.0%)	122 (3.3%)	160 (4.3%)	589 (15.9%)	143 (3.9%)	23 (0.6%)	138 (3.7%)	106 (2.9%)
<del>4</del>	CSIRO-Mk3-										
<del>3</del>	6-0										

5	GFDL-CM3	1246	749 (60.1%)	150 (12.1%)	68 (5.4%)	41 (3.3%)	113 (9.1%)	52 (4.2%)	5 (0.4%)	44 (3.6%)	19 (1.5%)
6	GISS-E2-H	1699	1045 (61.5%)	252 (14.8%)	109 (6.4%)	96 (5.7%)	94 (5.5%)	71 (4.2%)	4 (0.3%)	22 (1.3%)	5 (0.3%)
7	GISS-E2-R	1678	1035 (61.7%)	238 (14.2%)	92 (5.5%)	90 (5.4%)	103 (6.1%)	86 (5.1%)	4 (0.2%)	23 (1.4%)	5 (0.3%)
8	HadGEM2-CC	8186	3124 (38.2%)	593 (7.2%)	403 (4.9%)	826 (10.1%)	359 (4.4%)	2278 (27.8%)	264 (3.2%)	196 (2.4%)	142 (1.7%)
9	HadGEM2-ES	7973	3221 (40.4%)	579 (7.3%)	418 (5.2%)	820 (10.3%)	321 (4.0%)	1988 (24.9%)	340 (4.3%)	144 (1.8%)	139 (1.7%)
10	MIROC4h	735	437 (59.4%)	71 (9.7%)	81 (11.1%)	45 (6.1%)	64 (8.8%)	9 (1.2%)	0.1 (0.02%)	3 (0.5%)	24 (3.2%)
11	MIROC5	2716	1762 (64.9%)	269 (9.9%)	175 (6.5%)	96 (3.5%)	243 (8.9%)	26 (1.0%)	4 (0.2%)	79 (2.9%)	61 (2.2%)
12	MIROC-ESM	3339	2627 (78.7%)	244 (7.3%)	72 (2.2%)	30 (0.9%)	273 (8.2%)	0.6 (0.02%)	0.3 (0.008%)	89 (2.6%)	6 (0.2%)
13	MIROC-ESM-CHEM	3598	2719 (75.6%)	274 (7.6%)	84 (2.3%)	44 (1.2%)	362 (10.1%)	1 (0.03%)	0.4 (0.01%)	100 (2.8%)	13 (0.4%)
14	MRI-CGCM3	2107	1146 (54.4%)	258 (12.2%)	22 (1.1%)	174 (8.3%)	390 (18.5%)	55 (2.6%)	2 (0.09%)	49 (2.3%)	11 (0.5%)
15	MRI-ESM1	2052	1108 (54.0%)	246 (12.0%)	21 (1.0%)	167 (8.1%)	392 (19.1%)	57 (2.8%)	2 (0.09%)	48 (2.3%)	10 (0.5%)
16	MERRA-2	1670	1104 (61.1%)	182 (16.2%)	56 (7.7%)	55 (3.1%)	162 (6.3%)	59 (2.6%)	8 (0.5%)	30 (1.7%)	15 (0.7%)

1229 **Table 5.** Total dust deposition and wet deposition in the global surface, continents,  
 1230 and oceans, respectively from CMIP5 models and MERRA-2 reanalysis. Only the  
 1231 seven CMIP5 models with both dry and wet depositions provided are used here.

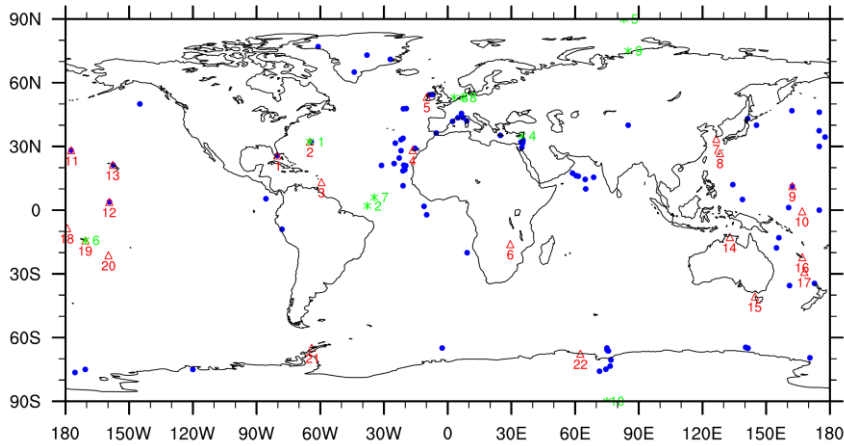
Model	Global		Continent		Ocean	
	Total	Wet <sup>a</sup>	Total <sup>b</sup>	Wet <sup>a</sup>	Total <sup>b</sup>	Wet <sup>a</sup>
ACCESS1-0	2216	261 (12%)	2019 (91%)	159 (8%)	197 (9%)	102 (52%)
<u>MRI-CGCM3</u>	<u>2109</u>	<u>819 (39%)</u>	<u>1649 (78%)</u>	<u>499 (30%)</u>	<u>460 (22%)</u>	<u>319 (69%)</u>
<u>MRI-ESM1</u>	<u>2054</u>	<u>801 (39%)</u>	<u>1609 (78%)</u>	<u>492 (30%)</u>	<u>445 (22%)</u>	<u>309 (69%)</u>
CanESM2	2965	882 (30%)	2279 (77%)	513 (22%)	686 (23%)	369 (54%)
CESM1-CAM5	3454	1243 (36%)	2850 (83%)	945 (33%)	604 (17%)	298 (49%)
GISS-E2-H	1684	641 (38%)	1359 (81%)	410 (30%)	324 (19%)	231 (71%)
GISS-E2-R	1665	625 (37%)	1331 (80%)	392 (29%)	334 (20%)	232 (70%)
<del>MRI-CGCM3</del>	<del>2109</del>	<del>819 (39%)</del>	<del>1649 (78%)</del>	<del>499 (30%)</del>	<del>460 (22%)</del>	<del>319 (69%)</del>
<del>MRI-ESM1</del>	<del>2054</del>	<del>801 (39%)</del>	<del>1609 (78%)</del>	<del>492 (30%)</del>	<del>445 (22%)</del>	<del>309 (69%)</del>
MERRA-2	1792	692 (38.6%)	1272 (71%)	335 (26%)	520 (29%)	356 (69%)

1232 <sup>a</sup>: The ratio of wet deposition to total deposition is given in parenthesis next to wet  
 1233 deposition.

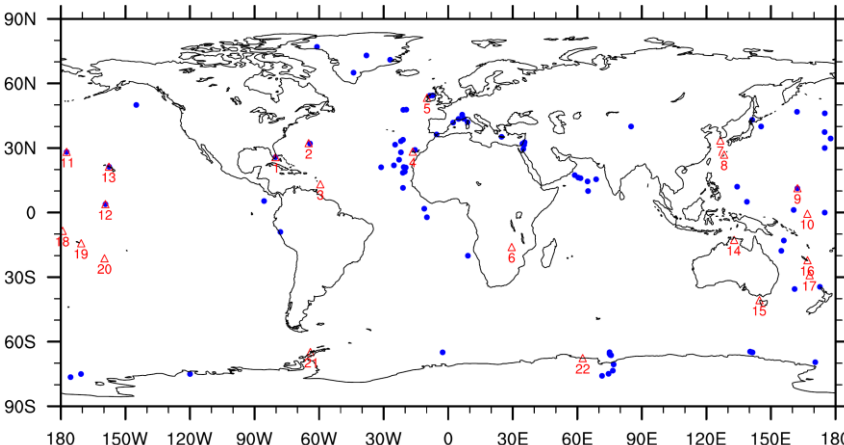
1234 <sup>b</sup>: The fraction of continental (or oceanic) deposition to global deposition is given in  
 1235 next to continental (or oceanic) deposition.

1236

1237



1238



1239

1240 **Figure 1.** The distribution of observational stations used in this study: blue circles for  
1241 dust deposition and, red triangles for surface dust concentrations, and green asterisks  
1242 for fraction of wet deposition. The descriptions of all these stations can be found in  
1243 Section 3.1.

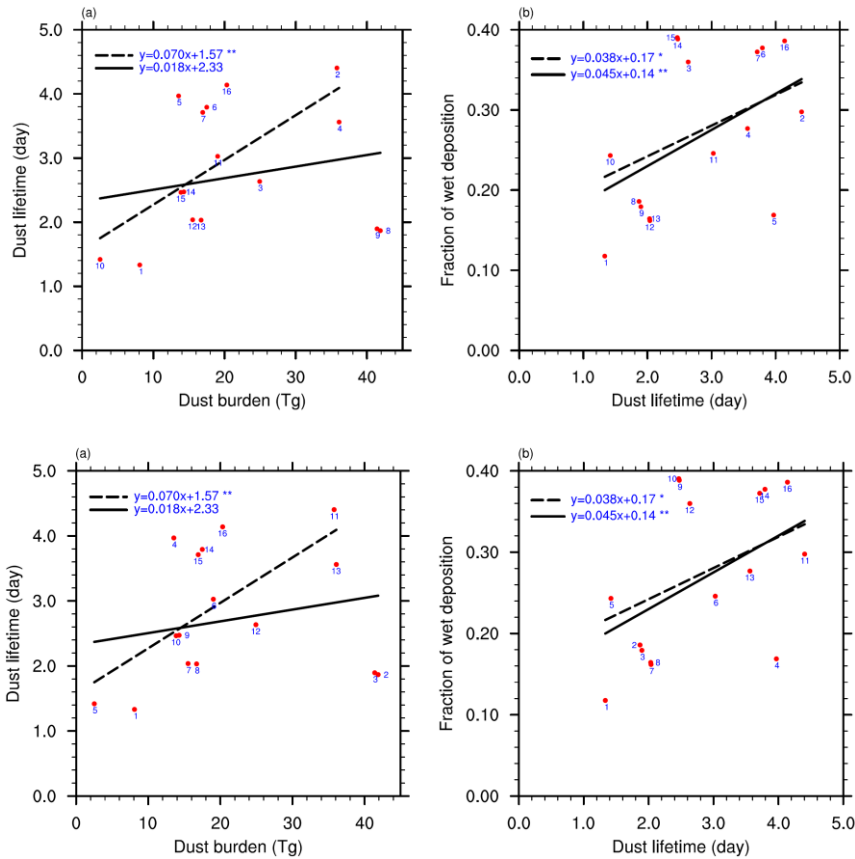
1244



1245

1246

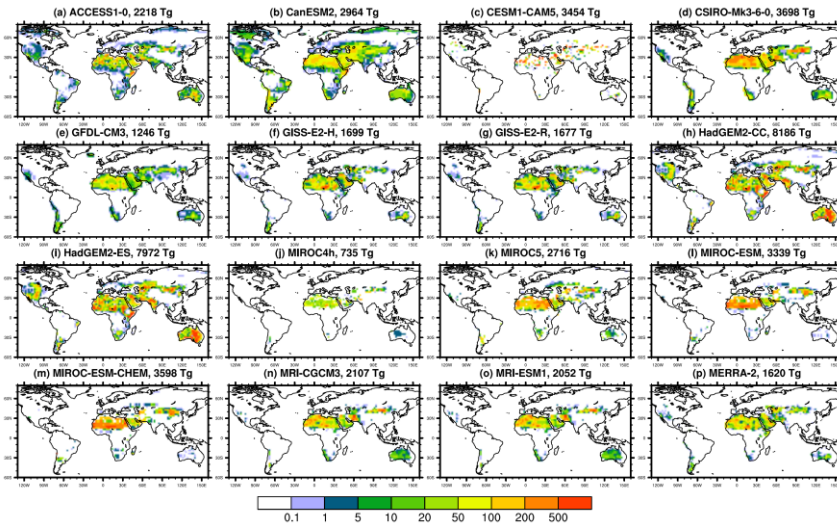
1247



1248 **Figure 2.** Scatter plot of (a) dust burden versus dust life time and (b) dust life time  
1249 versus fraction of wet deposition to total deposition in 15 CMIP5 models and in  
1250 MERRA-2 reanalysis. The models are indexed as Table 1. The regression lines from  
1251 all the CMIP5 models (solid) and the CMIP5 models excluding HadGEM2-CC/ES  
1252 models (dash) are also shown with the slopes and intercepts for the regression  
1253 equation. Significant test for each regression is denoted by one asterisk (\*; above  
1254 significant level of 0.1) and two asterisks (\*\*; above significant level of 0.05) after  
1255 each regression equation.

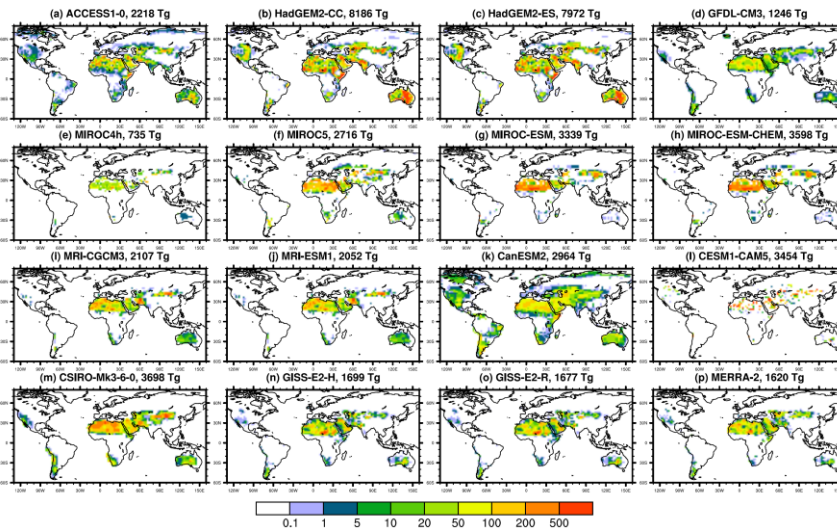
1256

1257



1258

1259



1260

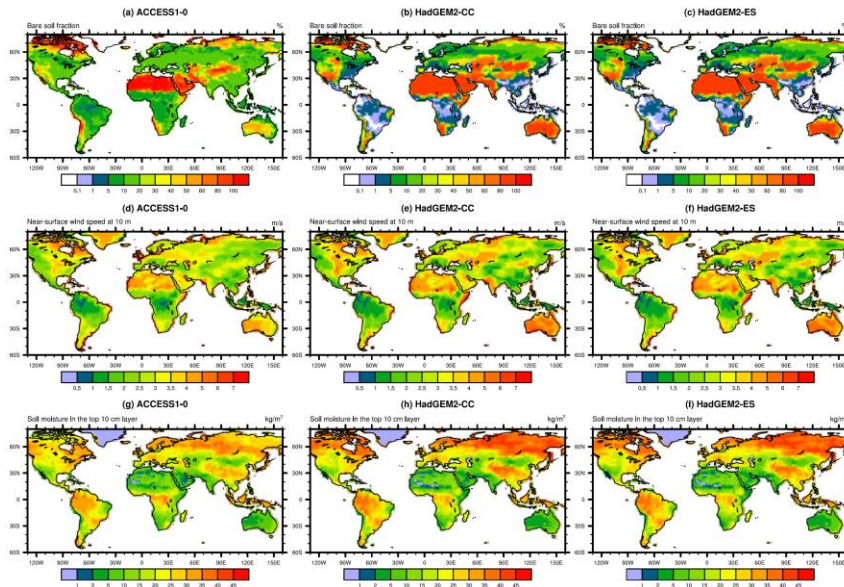
1261 **Figure 3.** (a-o) Annual mean dust emission flux ( $\text{g m}^{-2} \text{yr}^{-1}$ ) during 1960-2005 from

1262 15 CMIP5 models, and (p) annual mean dust emission ( $\text{g m}^{-2} \text{yr}^{-1}$ ) during 1980-2018

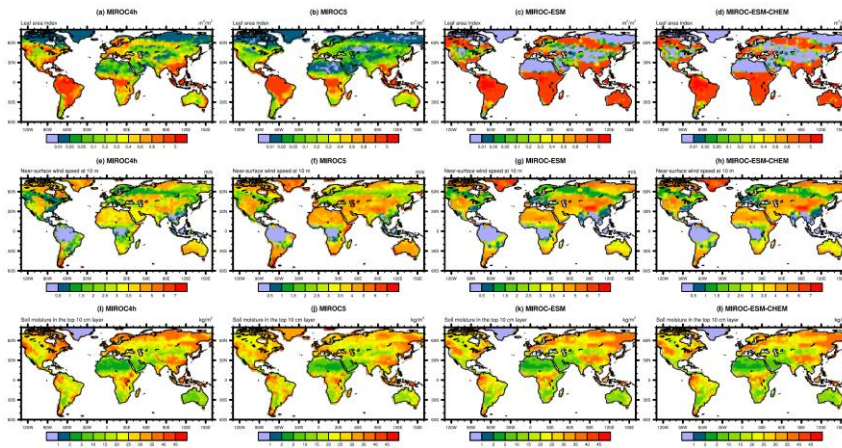
1263 from MERRA-2 reanalysis. The total annual global dust emission is included in the

1264 title of each panel.

1265



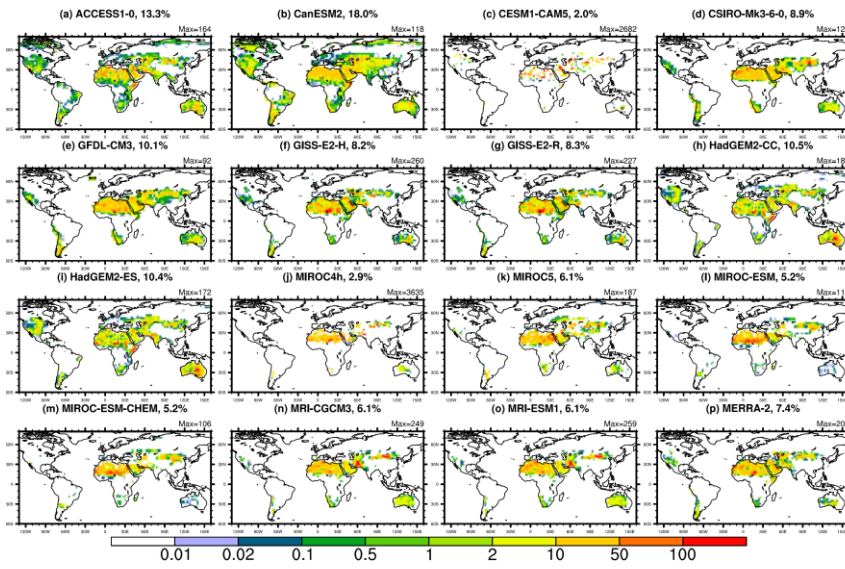
1266  
 1267 Figure 4. Bare soil fraction (%), near-surface wind speed at 10 m over land ( $m s^{-1}$ ),  
 1268 soil moisture in the top 10 cm layer ( $kg m^{-2}$ ) in ACCESS1-0, HadGEM2-CC, and  
 1269 HadGEM2-ES. Note that except bare soil fraction in ACCESS1-0 which is prescribed  
 1270 and set constant for each year, other results are all from model simulations during  
 1271 1960-2005.  
 1272



1273

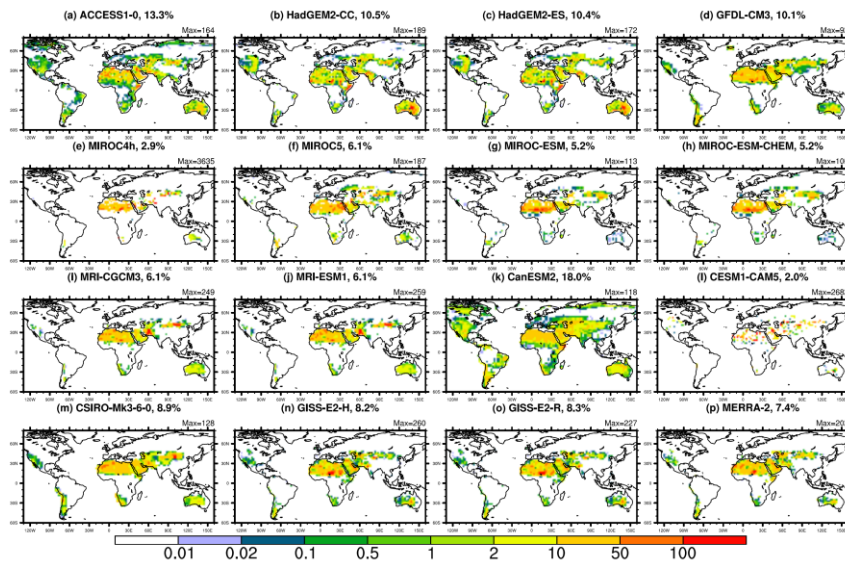
1274 Figure 5. Minimum leaf area index of a calendar year ( $\text{m}^2 \text{m}^{-2}$ ), annual mean surface  
 1275 wind speed at 10m ( $\text{m s}^{-1}$ ), and mean soil moisture in the top 10 cm layer ( $\text{kg m}^{-2}$ )  
 1276 during 1960-2005 in four MIROC family models. For each grid box, monthly mean  
 1277 leaf area index for each month of a calendar year is first derived based on the average  
 1278 of 1960-2005, and then the minimum of leaf area index among these months (i.e.,  
 1279 January to December) is plotted.

1280



1281

1282



1283

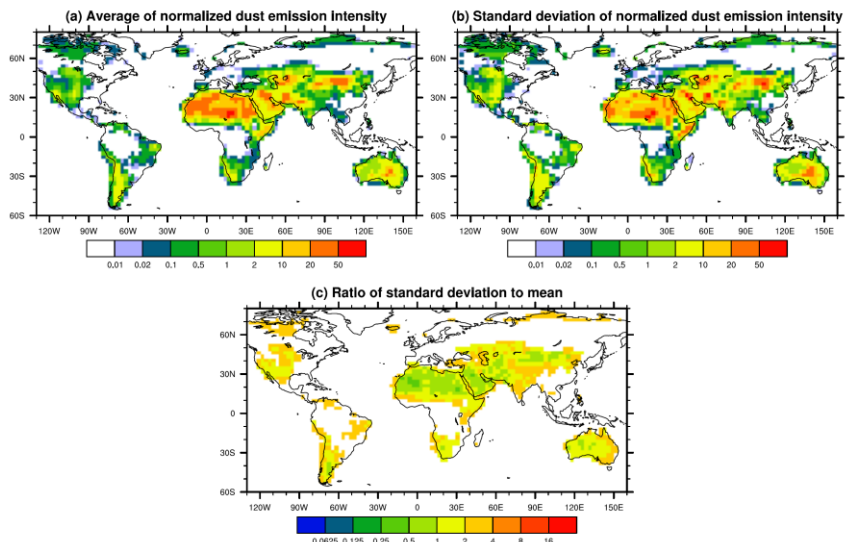
1284

1285

1286

**Figure 46.** Normalized dust emission flux in 15 CMIP5 models and MERRA-2 reanalysis. Normalized dust emission flux is calculated from dust emission flux divided by global mean for each model. The percentage of dust source area relative to

1287 global total surface area is given in the title of each panel. Dust source area is defined  
1288 as the normalized dust emission flux greater than 0.01. The maximum normalized  
1289 dust emission flux is also given in the top right corner of each panel.  
1290



1291

1292

**Figure 57.** Mean, standard deviation, and relative standard deviation (also known as coefficient of variation) of normalized dust emission flux from 15 CMIP5 models.

1293

1294

Relative standard deviation is derived by calculating the ratio of standard deviation to mean.

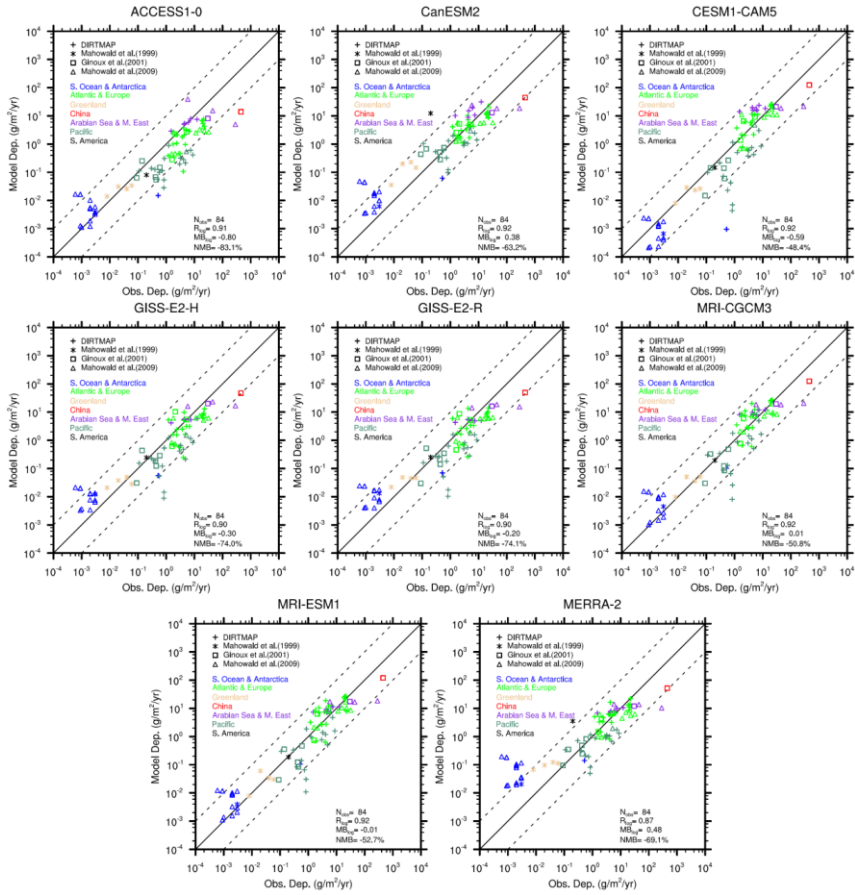
1295

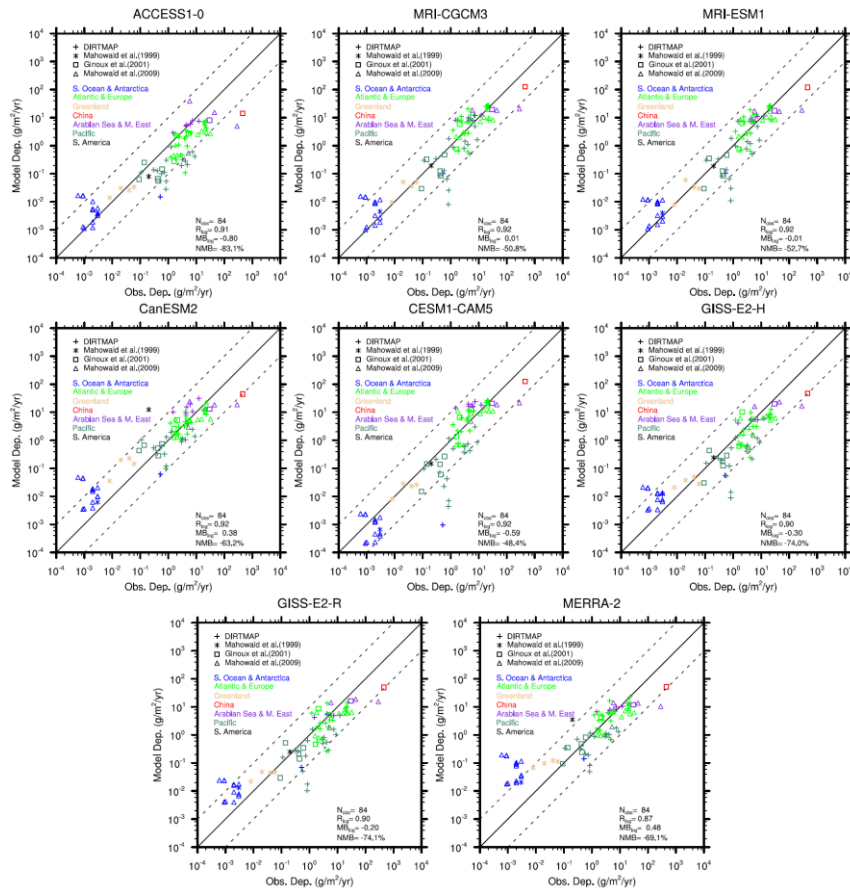
1296

1297

65

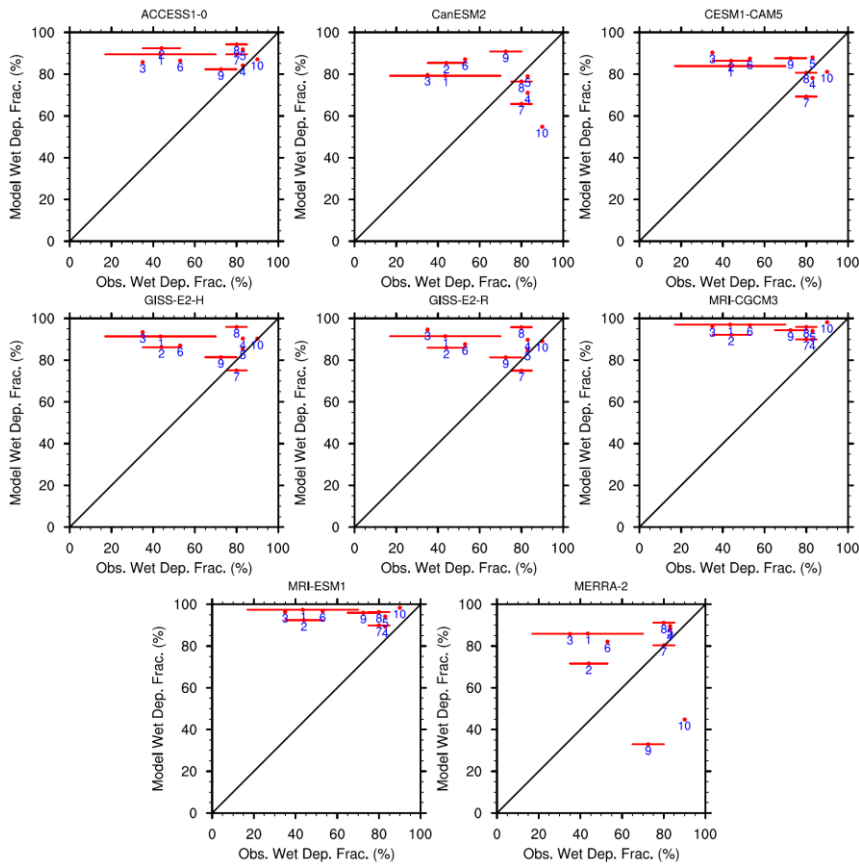






1299  
 1300 **Figure 68.** Scatterplot of dust deposition flux at 84 selected stations between models  
 1301 and observations. The stations are marked with different styles according to the  
 1302 sources of data and with different colors for different locations (Section 3). Also given  
 1303 are the correlation coefficients and mean bias between models and observations (after  
 1304 taking the logarithms;  $R_{log}$  and  $MB_{log}$ , respectively). The normalized mean bias (NMB)  
 1305 that is calculated from the mean bias divided by mean observations is given as well.  
 1306 The 1:1 (solid) and 1:10/10:1 (dash) lines are plotted for reference.

1308

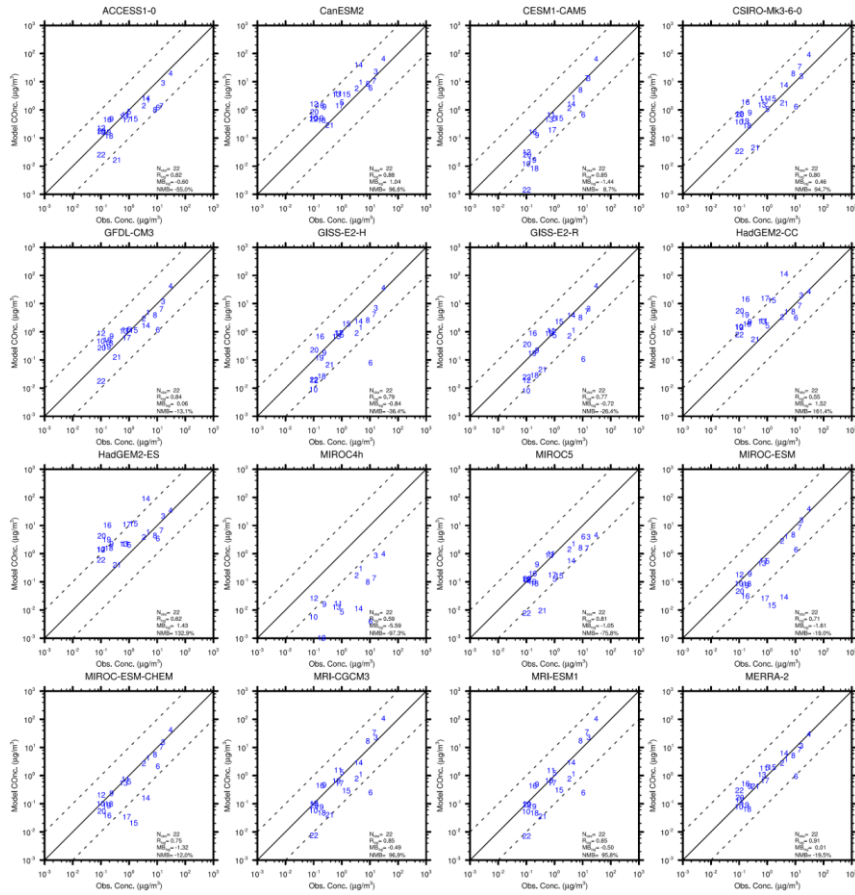


1309

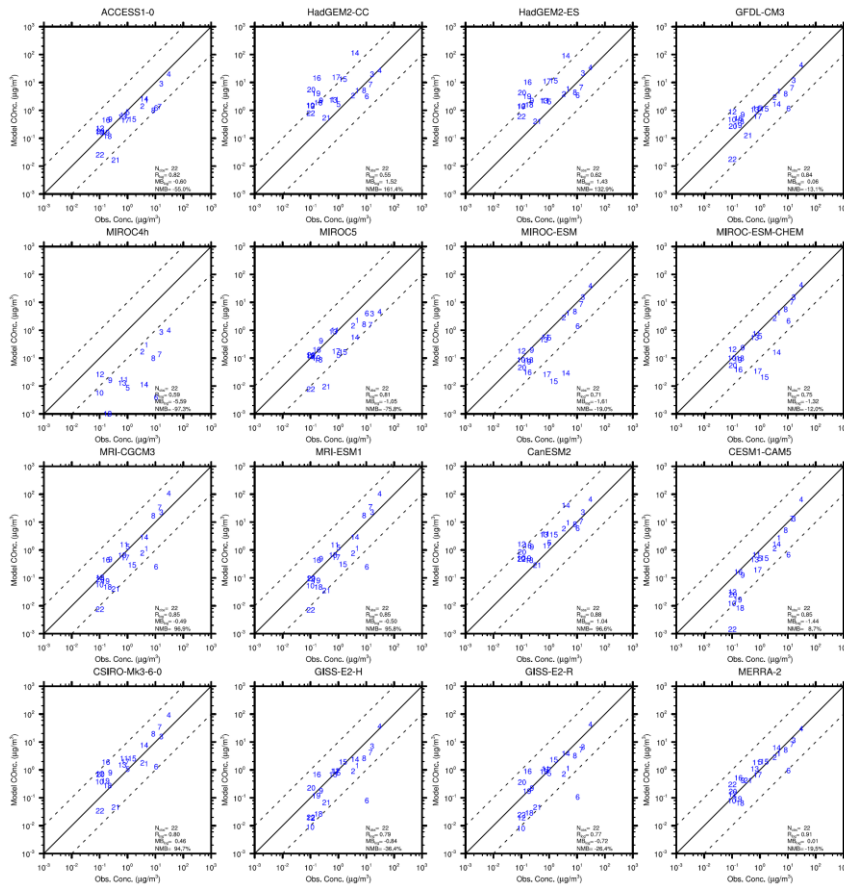
1310 **Figure 7.** Scatterplot of fraction of wet deposition in total deposition between models  
1311 and observations. For the observations that provide the minimum and maximum  
1312 values, the mean of minimum and maximum values is used with the ranges indicated  
1313 by a horizontal line. Station numbers are indexed following Table 2.

1314

1315



1316



1317  
 1318 **Figure 89.** Scatterplot of surface dust concentration at 22 selected stations between  
 1319 models and observations. The stations are indexed as Table 2 and their locations are  
 1320 shown in Figure 1. Also given are the correlation coefficients and mean bias between  
 1321 models and observations (after taking the logarithms;  $R_{\log}$  and  $MB_{\log}$ , respectively).  
 1322 The normalized mean bias (NMB) that is calculated from the mean bias divided by  
 1323 mean observations is given as well. The 1:1 (solid) and 1:10/10:1 (dash) lines are  
 1324 plotted for reference. The comparison results for some stations (#15-17 and #19-22  
 1325 for MIROC4h; #21 and #22 for MIROC-ESM and MIROC-ESM-CHEM) are not  
 1326 shown as they are located too low and outside the frame.